NASA CR-137,917

# APPLICATION OF THE ADAPTIVE-WALL CONCEPT TO THREE-DIMENSIONAL LOW-SPEED WIND TUNNELS

By J. C. Erickson, Jr.

September 1976





Prepared under Contract No. NAS2-8777 by
Calspan Corporation
Buffalo, New York

for

AMES RESEARCH CENTER
NATIONAL AERONAUTICS AND SPACE ADMINISTRATION

| 1. Report No. | 2. Government Accession No. | 3. Recipient's Catalog No. |
|---|---|---|
| NASA CR-137,917 | | |

| 4. Title and Subtitle | 5. Report Date |
|---|---|
| Application of the Adaptive-Wall Concept to Three-Dimensional Low-Speed Wind Tunnels | September 1976 |
| | 6. Performing Organization Code |
| 7. Author(s) | 8. Performing Organization Report No. |
| J.C. Erickson, Jr. | RK-5717-A-1 |
| | 10. Work Unit No. |
| 9. Performing Organization Name and Address | 11. Contract or Grant No. |
| Calspan Corporation<br>P.O. Box 235<br>Buffalo, New York 14221 | NAS2-8777 |
| | 13. Type of Report and Period Covered |
| 12. Sponsoring Agency Name and Address | Contractor Report |
| National Aeronautics and Space Administration<br>Ames Research Center<br>Moffett Field, California 94035 | 14. Sponsoring Agency Code |
| 15. Supplementary Notes | |

16. Abstract

Interference-free flows about a model in a wind tunnel exist when certain functional relationships are satisfied among disturbance velocity components at a measurement control surface located within the tunnel near, or at, the walls. These functional relationships are derived for three-dimensional subcritical flow fields in which no propulsion-system efflux intersects the control surface until far downstream. Three methods for evaluating the functional relationships have been developed. The first of these, the original multipole expansion (MPE) procedure, is based on a series of point singularities which satisfy the governing Prandtl-Glauert equation. The second, the modified MPE, provides an improved representation of finite-span wings and thereby extends the range of validity of the original MPE to larger ratios of span-to-control-surface-width. The third method is more general and is based on source distributions over the control surface. Several numerical examples are presented to help establish the range of validity of these evaluation methods. An accuracy-assessment procedure, which combines the original MPE procedure with classical wall-correction theory, has been developed to estimate the degree of interference at the model if the functional relationships are not satisfied exactly. Several numerical examples of this procedure are presented for representative wings and bodies.

| 17. Key Words (Suggested by Author(s)) | 18. Distribution Statement |
|---|---|
| Self-Correcting Wind Tunnels<br>Adaptive-Wall Wind Tunnels<br>V/STOL Wind Tunnels<br>Wind Tunnel Wall Interference | |

| 19. Security Classif. (of this report) | 20. Security Classif. (of this page) | 21. No. of Pages | 22. Price* |
|---|---|---|---|
| Unclassified | Unclassified | 75 | |

*For sale by the National Technical Information Service, Springfield, Virginia 22151

CONTENTS

# APPLICATION OF THE ADAPTIVE-WALL CONCEPT TO THREE-DIMENSIONAL LOW-SPEED WIND TUNNELS

By J. C. Erickson, Jr.
Calspan Corporation

## SUMMARY

Interference-free flows about a model in a wind tunnel exist when certain functional relationships are satisfied among disturbance velocity components at a measurement control surface located within the tunnel near, or at, the walls. These functional relationships are derived for three-dimensional subcritical flow fields in which no propulsion-system efflux intersects the control surface until far downstream. Three methods for evaluating the functional relationships have been developed. The first of these, the original multipole expansion (MPE) procedure, is based on a series of point singularities which satisfy the governing Prandtl-Glauert equation. The second, the modified MPE, provides an improved representation of finite-span wings and thereby extends the range of validity of the original MPE to larger ratios of span-to-control-surface-width. The third method is more general and is based on source distributions over the control surface. Several numerical examples are presented to help establish the range of validity of these evaluation methods.

An accuracy-assessment procedure, which combines the original MPE procedure with classical wall-correction theory, has been developed to estimate the degree of interference at the model if the functional relationships are not satisfied exactly. Several numerical examples of this procedure are presented for representative wings and bodies.

# INTRODUCTION

The flow fields about helicopters and other V/STOL aircraft are highly complex and are difficult both to simulate in a wind tunnel and to predict analytically. Many V/STOL designs incorporate integrated lift and propulsion systems that are characterized by a high-energy efflux which is deflected downward at a large angle to the direction of flight in order to generate lift at low flight speeds. Flight speeds of these vehicles range from hover, or near hover, through transition to cruise flight, so that the disturbance velocities introduced by the vehicles, including their propulsion systems, are comparable to, or even greater than, the flight velocity over an important operating range. Thus, in wind-tunnel testing of V/STOL aircraft, the presence of the tunnel boundaries causes larger interference effects than exist for comparably-sized conventional aircraft with their relatively smaller flow disturbance velocities. The necessity for large wind-tunnel models is indicated to minimize scaling effects, which are not well understood, and to facilitate modeling the propulsion systems, especially those with high disk loadings such as fans and jets. These considerations, in part, have led to the requirements for even larger testing facilities (ref. 1).

The concept of wind-tunnel-boundary corrections in solid-wall and open-jet tunnels for conventional aircraft configurations in subsonic, subcritical flight generally has proved adequate. This results principally because the aircraft generates only small disturbances in the flow, including a trailing vortex system due to lift which does not deflect significantly from the direction of flight. These vehicles and the wall boundary conditions then can be represented analytically by linearized aerodynamic theory with all its powerful techniques and connotations, e.g., superposition. Therefore, boundary-induced corrections to the incident flow can be interpreted in terms of corrections to the measured aerodynamic characteristics of the vehicle, making use of the extensive knowledge of the general aerodynamic behavior of this class of configurations. The idea of corrections becomes less viable for conventional aircraft configurations in ventilated tunnels, especially as the flight speed

becomes transonic with larger flow disturbances, loss of superposition, uncertainty in the form of the wall boundary conditions, and flow fields that cannot be predicted accurately.

The concept of tunnel-boundary corrections for helicopters and V/STOL aircraft also rests on a less than satisfactory basis. The propulsion-system efflux often interacts strongly with the rest of the aircraft and generates a highly-deflected trailing-vortex system which may also interact with the tunnel boundaries. Also, as mentioned above, the flow disturbance velocities introduced by the vehicle may be comparable to, or greater than, the flight velocity at low speeds near hover and during transition. Therefore, these vehicles cannot be represented adequately by linearized aerodynamic models and so superposition is no longer valid. As a result, the unconfined-flow aerodynamic characteristics are not well understood and cannot be predicted as well as for conventional aircraft. Therefore, even if tunnel-boundary-induced velocity disturbances to the incident flow can be estimated accurately, their interpretation in terms of the measured aerodynamic characteristics may not be possible. Finally, the basic nature of the flow in the tunnel may bear no relationship whatsoever to the flow field in free flight, as shown first by Rae (ref. 2). That is, there may be a flow breakdown consisting of a recirculation of the propulsion-system efflux upstream and around the tunnel walls. Flow breakdown occurs in a given tunnel, for a given vehicle configuration, below some minimum tunnel speed (refs. 2-8). In view of these considerations, tunnel-boundary effects and corrections for them are not in a fully satisfactory state for helicopter and V/STOL testing.

The difficulties in wind-tunnel testing of V/STOL configurations have motivated considerable research in recent years. These efforts have followed three rather broad lines. First has been the development of theoretical methods for calculating boundary-induced interference-velocity distributions within the test section. These methods are in the spirit of classical tunnel-boundary-correction theory and are based on simplified analytical representations of various tunnel-wall and vehicle configurations including the propulsion-system efflux. Some of the principal contributions to this line of development

have been by Heyson (refs. 9-12), Lo, Binion and Kraft (refs. 13-17), and Joppa (ref. 18). Second are the experimental investigations which have examined the nature of the interference on representative models and on the nature of the flow within the test section. These investigations (refs. 2-8) discovered the existence of flow breakdown and have examined the conditions for its occurrence. Finally, the third area of research on tunnel-boundary effects is an outgrowth of the theoretical calculation of interference-velocity distributions. This research is aimed at the development of test-section geometrical configurations which minimize the interference velocities and/or make them more nearly uniform over the complete extent of typical models, so that corrections can be made for any residual wall effects (refs. 13-15, 19-20). The validity of these test-section configurations relies on the ability to represent analytically the vehicle, its propulsion system, and the characteristics of flow through ventilated walls. Consequently, the results of these studies serve principally as guides to the objective of low-interference tunnels. Thus, they have been augmented by experimental investigations with similar objectives (refs. 21-28). Notable among these latter investigations are those of Kroeger and Martin (refs. 21-22) and of Bernstein and Joppa (refs. 27-28) because they introduce active control of the flow in the tunnel by applying blowing and suction through ventilated tunnel walls. Their wall-control requirements are determined from computations of the flow field near the walls by means of a theoretical representation of the geometrical configuration to be tested. Therefore, their method can be only as good as their ability to predict this model flow field accurately. Hence, for complicated V/STOL models over a large portion of their flight envelope, this can be an important limitation.

The approaches just described hold promise for developing V/STOL test-section configurations with low levels of boundary interference. Nevertheless, each tunnel design is tied closely to a specific vehicle configuration and size, so that generalization is difficult. Even more important, there is no way, other than to test the same model in a larger (and therefore, supposedly interference-free) tunnel, to verify that the boundary interference actually has been eliminated. A further, and significant, conceptual step which removes

some of these restrictions is the self-correcting, or adaptive-wall, wind tunnel proposed by Sears (ref. 29). The self-correcting tunnel concept, which is described more fully in the Appendix, also uses active control of the flow at the tunnel walls. In addition, however, measurements of flow disturbance quantities at a suitable control surface within the tunnel are combined, in iterative fashion, with the evaluation of appropriate functional relationships. Satisfaction of the functional relationships by the measured flow disturbance quantities assures that the flow about the model is interference free.

Application of the adaptive-wall concept to transonic wind tunnels is being pursued actively by several groups at this time, see references 29 to 36. In particular, an experimental demonstration of the fully implemented concept, as applied to a two-dimensional transonic tunnel, is being carried out in the Calspan One-Foot Wind Tunnel. In this tunnel, active wall control is achieved by segmenting the plenum surrounding the porous walls, and controlling the flow through the walls by applying suction or pressure to the plenum segments. Important progress to date on this work is reported in references 29 to 31.

For low speeds as well, the ultimate embodiment of the adaptive-wall concept would have the capability to guarantee an interference-free flow in the test section for any V/STOL configuration and attitude with respect to the free stream. Thus, the concept incorporates the following considerations. Unconfined flow about an arbitrary V/STOL configuration certainly cannot be calculated with sufficient accuracy that wind-tunnel testing can be eliminated. On the other hand, the boundaries of a wind tunnel can cause so much interference with the flow about a model that the test results may be in question, especially at very low free-stream speeds. Although the flow field in the vicinity of the model cannot be predicted analytically, the flow field external to the control surface is represented by a well-posed boundary-value problem that is within the capability of existing analytical and computational techniques. Therefore, by combining theory and experiment in a way that uses each to its best advantage, the self-correcting wind tunnel offers the prospect of simulation of free-flight conditions in the flow about the model.

The adaptive-wall wind tunnel concept can also be applied to testing in existing conventional tunnels without provisions for flow control by the walls. In this application, measurements still would be made at a suitable control surface in the tunnel, and the unconfined-flow functional relationships would be evaluated for each test, just as described. If the functional relationships were found to be satisfied to within some specified accuracy, the test could be considered effectively unconfined by the walls so that the data could be considered interference free. If, on the other hand, the functional relationships were not satisfied to the specified accuracy, the data would contain interference effects. Carrying this idea a step further, the self-correcting concept could even provide a basis for improved techniques for computing wall-interference corrections, when such corrections are meaningful.

We thus see that by means of measurements and evaluations of functional relationships, the basic self-correcting tunnel concept can be used to establish criteria for the accuracy of tests without wall control. Irrespective of which mode of operation is selected, i.e., elimination of interference or evaluation of the degree of interference present, many of the theoretical and measurement techniques which must be investigated are identical. Therefore, the initial research reported here is applicable either to the development of a complete self-correcting V/STOL tunnel or to the use of measurements and functional relationships as an indication of interference-free conditions in existing tunnels.

In the next section, the functional relationships that must be satisfied in wall-interference-free flow are established for conventional three-dimensional models, for which no propulsion-system efflux intersects the measurement control surface until far downstream. Evaluation of the functional relationships for conventional models by means of two techniques, namely multipole expansion (MPE) procedures and a source distribution method, are described along with typical results for models both in and out of ground effect. The question of assessing the accuracy required in satisfying the unconfined-flow functional relationships, as far as the interference on the wind-tunnel model is concerned, is discussed in the following section. A procedure for such an accuracy

assessment is developed using conventional tunnel-interference theory together with flow measurements and use of the MPE technique for evaluating the functional relationships. Several examples are given which show permissible amounts of departure from the exact evaluation of the functional relationships. Finally, conclusions are given for this first step in the investigation of the self-correcting wind tunnel concept for V/STOL testing.

## SYMBOLS

$AR$ aspect ratio, $4 b_w^2 / S_w$

$a$ half-width of control surface (see figure 1)

$b$ half-height of control surface (see figure 1)

$b_b$ half-length of body

$b_v$ semispan of horseshoe vortex in modified multipole expansion

$b_w$ semispan of wing

$C_D$ drag coefficient, $F_D / q_\infty S_w$

$C_L$ lift coefficient, $F_L / q_\infty S_w$

$C_p$ pressure coefficient, $p / q_\infty$

$C_1$ source strength in accuracy-assessment method (see equation (47))

$C_2$ infinitesimal-span horseshoe vortex strength in accuracy-assessment method (see equation (48))

$C_3$ doublet strength in accuracy-assessment method (see equation (49))

$c$ wing chord in two-dimensional flow (see figure 16)

$D$ function defined in Table I

$F_D$ drag force

$F_L$ lift force

$H_1, H_2, H_3$ functions defined in Table I

$h$ control-surface location in two-dimensional flow (see figure 16)

$h_g$ height of model above ground (see figures 12 and 13)

$J$ number of terms in multipole expansion

$M_\infty$ freestream Mach number

$N_j$ coefficient of $j^{th}$ term in multipole expansion of $v_{n_m}$ (see equation (31))

$n$ coordinate normal to control surface (see figure 1)

$p$ static pressure disturbance

$q_\infty$ freestream dynamic pressure, $\rho_\infty U_\infty^2/2$

$R$ distance from origin to point on control-surface cross section (see figure 1)

$\hat{R}$ function defined in Table I

$r$ distance from control surface to field point (see equation (23))

$S$ control surface at which flow disturbance measurements are made (see figures 1, 15 and 16)

$S_\omega$ reference area of model

$T$ function of diameter-to-length ratio of Rankine solid, given implicitly by $T = \tau(1+\tau^2 - T)^{1/4}$

$t$ coordinate tangential to control surface (see figure 1)

$U_\infty$ freestream velocity

$V_{n_j}, V_{t_j}$ normal, tangential components of velocity induced by $j^{th}$ multipole singularity of unit strength (see equations (39) and (40))

$V_{x_j}, V_{y_j}, V_{z_j}$ $x$, $y$, $z$ components of velocity induced by $j^{th}$ multipole singularity of unit strength (see Table I)

$V$ model volume

$v_n, v_t$ normal, tangential components of disturbance velocity

$v_x, v_y, v_z$ $x$, $y$, $z$ components of disturbance velocity

$X_j$ coefficient of $j^{th}$ term in multipole expansion of $v_{x_m}$ (see equation (28))

$x, y, z$ basic coordinate system (see figure 1)

$x_o, z_o$ offset of center of model from origin

$Y, Z$ coordinate of control-surface cross section

$\hat{y}, \hat{z}$ functions defined in Table I

$\alpha$ model angle of attack

$\alpha_o$ effective model angle of attack due to parabolic-arc camber

$\beta$ $(1-M_\infty^2)^{1/2}$

$\Gamma_v$ strength of horseshoe vortex in modified multipole expansion (see equation (41))

$\Delta_n(), \Delta_x()$ wall-interference correction to quantity ( ) based on $v_{n_m}, v_{x_m}$ boundary conditions

$\theta$ polar angle of point on control-surface cross section (see figure 1)

$\hat{\theta}$ eccentric angle of point on elliptical control-surface cross section (see equation (7))

$\theta_c$ polar angle of corner of rectangular control-surface cross section (see equation (9))

$\rho_\infty$ freestream density

$\sigma$ strength of source distribution on control surface

$\tau$ diameter-to-length ratio of Rankine solid

$\Phi$ acceleration potential

$\phi$ disturbance velocity potential

$\bar{\phi}$ idealized disturbance velocity potential of model in unconfined flow

$\phi^*$ interference disturbance velocity potential induced by tunnel boundaries

$\psi$ angle between $n$ and $z$ axes for control surface (see figure 1)

Subscripts:

$c$ calculated by evaluation of functional relationships

$j$ index of term in multipole expansion

$m$ measured at control surface

$\infty$ free stream

## EXTERNAL-FLOW FUNCTIONAL RELATIONSHIPS

### Control-Surface Geometry

The functional relationships which must be satisfied among the measured flow disturbance quantities in order for unconfined-flow conditions to exist in a flow will be discussed with respect to figure 1. This figure describes a flow with free stream speed $U_\infty$ in the $x$-direction about a body located near the origin of a rectangular $x$, $y$, $z$ coordinate system. We are concerned principally with the flow field external to the control surface $S$ which encloses the body. Only part of the control surface is shown in figure 1 because it is assumed to extend infinitely far upstream and downstream with a uniform cross section. The question of the effect of truncating the control surface to a finite length is an important one, which must be considered ultimately. Answering this question requires a more detailed consideration of the flow field within the tunnel than has been considered here.

We assume that the cross section of the control surface can be expressed parametrically in terms of the angle $\theta$ by $y = Y(\theta)$ and $z = Z(\theta)$. The angle $\theta$ is measured conveniently from the $z$-axis, as shown in figure 1, because the $x$-$z$ plane is the plane of symmetry for most aircraft configurations in longitudinal flight. We assume further that the control surface is symmetrical about the $x$-$z$ and $x$-$y$ planes with width $2a$ and height $2b$ as shown. The coordinate $t$ tangent to the control surface is a curvilinear

coordinate in planes perpendicular to the $x$-axis and is positive in the sense of increasing $\theta$. The coordinate $n$ is the outward normal to the control surface and completes a right-handed $x$, $n$, $t$ coordinate system. Both $n$ and $t$ are functions of $\theta$ along with the angle $\psi$ between the $n$- and $z$-axes, which is given in terms of the geometry of figure 1 as

$$\psi(\theta) = \tan^{-1}(dz/dy) = \tan^{-1}\left[(dz/d\theta)/(dy/d\theta)\right] \tag{1}$$

The length $R$ is the distance from the origin to the surface and is also a function of $\theta$. The disturbance velocity components in the $x$, $n$ and $t$ directions along the control surface are defined as $v_x$, $v_n$ and $v_t$, respectively.

The shape of the control-surface cross section does not have to be the same as that of the wind tunnel itself, so there is considerable flexibility in the choice. The most convenient shape from a computational point of view is a circle, for which the control surface and the entire flow field can be expressed easily in terms of the cylindrical coordinates $x$, $r$, $\theta$. In this system, $a = b$, where $a$ becomes the radius, and so the control surface is defined by

$$y = -a \sin\theta \tag{2}$$

$$z = a \cos\theta \tag{3}$$

and so,

$$\psi = \theta \tag{4}$$

Unfortunately, there are two important limitations for general testing with a circular cross section. First, it could limit unnecessarily the allowable model size in a rectangular or oval tunnel because the largest dimension of the model normal to the $x$-axis can be no larger than the diameter of the control surface. For example, in a rectangular tunnel with a height-to-width ratio $b/a$ less than one, the span of a wing would have to be limited to

the tunnel height, as shown in the sketch. For this geometry, the maximum model size would be unduly limited, especially for a fully-implemented self-correcting configuration in which the model could be larger than is acceptable in a conventional tunnel. The second limitation concerns the self-correcting tunnel simulation of ground effect. The ground plane must lie outside the control surface and so for a wing with a circular control-surface cross section, the maximum height above ground would be unrealistically limited to a wing semispan. We conclude, therefore, that a better choice would be a control-surface cross section that is elongated in the direction of the maximum model dimension normal to the $x$-axis, for example, a rectangle, ellipse or another oval shape such as the cross sections of existing tunnels.

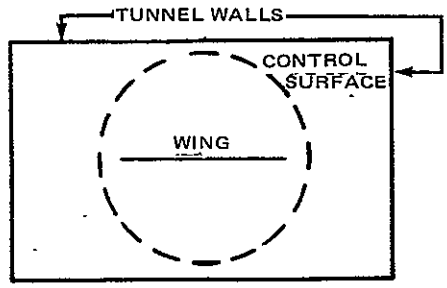


An elliptical control-surface cross section is defined by

$$y = -a \sin \hat{\theta} \tag{5}$$

$$z = b \cos \hat{\theta} \tag{6}$$

where $\hat{\theta}$ is the eccentric angle which is related to the polar angle $\theta$ of figure 1 by

$$\hat{\theta} = \tan^{-1}(b \tan \theta / a) \tag{7}$$

From equation (1) then, we find that

$$\psi = \tan^{-1}(b^2 \tan \theta / a^2) \tag{8}$$

The circular cross section is a special case of the ellipse, of course, with $a = b$ .

A rectangular control-surface cross section is defined as follows, where $-\pi < \theta \leq \pi$ and

$$\theta_c = \tan^{-1}(a/b) \tag{9}$$

For $\pi - \theta_c < \theta \leq \pi$, and also for $-\pi < \theta < -\pi + \theta_c$,

$$Y = b \tan\theta \tag{10}$$

$$Z = -b \tag{11}$$

$$\psi = \pi \tag{12}$$

For $-\pi + \theta_c < \theta < -\theta_c$,

$$Y = a \tag{13}$$

$$Z = -a \cot\theta \tag{14}$$

$$\psi = -\frac{\pi}{2} \tag{15}$$

For $-\theta_c < \theta < \theta_c$,

$$Y = -b \tan\theta \tag{16}$$

$$Z = b \tag{17}$$

$$\psi = 0 \tag{18}$$

For $\theta_c < \theta < \pi - \theta_c$,

$$Y = -a \tag{19}$$

$$Z = a \cot\theta \tag{20}$$

$$\psi = \frac{\pi}{2} \tag{21}$$

Separate subroutines implementing cross sections of both elliptical and rectangular shape have been developed and checked. In all the applications described below, however, only elliptical cross sections have been considered.

## General Formulation of Functional Relationships

The two-dimensional functional relationships can be formulated, in the absence of propulsion-system efflux exiting through the control surface, in terms of either source or vortex distributions along the control surface. Both formulations are equivalent and for unconfined flow lead to the direct integral relationships between the disturbance velocity components normal and tangential to the control surface that are given in the Appendix. In two-dimensional flow about a body in ground effect, the alternative formulations are equivalent as well, but lead in each case to different pairs of equations, one of which is an integral equation and the other an integral evaluation once the integral equation has been solved.

Similarly, the three-dimensional unconfined-flow functional relationships, in the absence of the efflux intersecting the control surface, can be formulated in several ways. If we assume that incompressible, inviscid flow is a suitable approximation for the region external to the control surface, the most familiar formulation is found by considering a source distribution $\sigma(x,\theta)$ over the entire control surface $S$, whereupon the disturbance velocity potential $\phi$ can be written at a general field point $(x, y, z)$, following Hess and Smith (refs. 37-39) as

$$\phi(x,y,z) = \int_{-\infty}^{\infty}\int_{0}^{2\pi} \frac{\sigma(x',\theta')\, R(\theta')\, \sec(\theta'-\psi')\, d\theta'\, dx'}{r} \tag{22}$$

where the primes denote the variables of integration and

$$r = \left\{(x-x')^2 + \left[y - Y(\theta')\right]^2 + \left[z - Z(\theta')\right]^2\right\} \tag{23}$$

The velocity components can be found by differentiating equation (22) with respect to the appropriate coordinate directions. If this is done in the $x$, $n$, $t$ system and the appropriate limits are taken, we have on the control surface,

$$v_x(x,\theta) = \frac{\partial \phi(x,\theta)}{\partial x} = \int_{-\infty}^{\infty}\int_{0}^{2\pi} \sigma(x',\theta') \left[\frac{\partial}{\partial x}\left(\frac{1}{r}\right)\right]_{\substack{y=Y(\theta)\\ z=Z(\theta)}} R(\theta') \sec(\theta'-\psi')\, d\theta'\, dx' \tag{24}$$

$$v_n(x,\theta) = \frac{\partial \phi(x,\theta)}{\partial n} = -2\pi\sigma(x,\theta) + \int_{-\infty}^{\infty}\int_{0}^{2\pi} \sigma(x',\theta') \left[\frac{\partial}{\partial n}\left(\frac{1}{r}\right)\right]_{\substack{y=Y(\theta)\\ z=Z(\theta)}} R(\theta') \sec(\theta'-\psi')\, d\theta'\, d \tag{25}$$

$$v_t(x,\theta) = \frac{\partial \phi(x,\theta)}{\partial t} = \int_{-\infty}^{\infty}\int_{0}^{2\pi} \sigma(x',\theta') \left[\frac{\partial}{\partial t}\left(\frac{1}{r}\right)\right]_{\substack{y=Y(\theta)\\ z=Z(\theta)}} R(\theta') \sec(\theta'-\psi')\, d\theta'\, dx' \tag{26}$$

The integrals in equations (24) and (26) must be evaluated in the Cauchy principal value sense.

If the normal velocity component $v_n$ is assumed to be known on the control surface from measurements, equation (25) is an integral equation of the second kind and represents the classical Neumann problem of potential theory. General numerical techniques have been developed, principally by Hess and Smith (refs. 37-39), to solve equation (25) for arbitrary three-dimensional configurations. Once this equation has been solved for $\sigma$, equations (24) and (26) can be evaluated to get the other components for comparison with their measured values. As an alternative to evaluating equation (26) for $v_t$, however, we note that once $v_x$ has been evaluated from equation (24), the potential $\phi$ can be found on the control surface by integration, namely

$$\phi(x,\theta) = \int_{-\infty}^{x} v_x(x',\theta)\, dx' \tag{27}$$

In establishing equation (27), we have made use of the fact that $\phi$ must vanish at infinity upstream for the flow about a three-dimensional configuration of

finite upstream extent. The circumferential component $v_t$ on the control surface follows immediately from equation (27) by differentiation with respect to $t$. Thus, $v_t$ can be calculated directly from $v_x$.

If the axial disturbance velocity component $v_x$ is assumed to be known on the control surface from measurements, then the potential $\phi$ can be evaluated on $S$ from equation (27) and $v_t$ can be found as well. In this situation, equation (22) for $\phi$ (as evaluated at $y = Y(\theta)$ and $z = Z(\theta)$) and equation (24) for $v_x$ are alternative integral equations of the first kind representing the Dirichlet problem of potential theory. These equations also could be solved numerically, in principle, although they have not been given much attention for general three-dimensional configurations (ref. 38) because of their relative unimportance in conventional aerodynamic applications. Once $\sigma$ has been found from solution of either equation (22) or equation (24), then $v_n$ can be evaluated from equation (25) and compared with its measured values.

We have seen, then, that if the measured values of either $v_n$ or $v_x$ are used as the boundary conditions for the exterior flow, $\sigma$ can be found and the other two components can be evaluated. If the measured values of $v_t$ alone are used as the boundary conditions, however, the problem is not properly posed. For example, if $v_t$ is integrated over $t$, it determines $\phi$ only up to an unknown function of $x$ and so additional information is required to formulate a Dirichlet problem. This point can be seen more clearly if we consider an axisymmetric flow field with a circular cross-section shape for the control surface. In this case, the circumferential component $v_t$ would be identically zero, and so its specification certainly does not provide sufficient information for determining the other two components. Therefore, it is clear that measured values of either $v_n$ or $v_x$ can be used as boundary conditions for evaluating the unconfined-flow functional relationships, but that measured values of $v_t$ cannot be used as boundary conditions. That is, measurements of $v_n$ and $v_x$ would provide the redundant data that are necessary for determining whether a flow field is unconfined. Apparently, then, measurement of $v_t$ is not required because its measured values must agree with the calculated values

if the measured and calculated values of $v_n$ and $v_x$ agree. Nevertheless, its retention provides an additional indication of the degree of satisfaction of the unconfined-flow conditions.

## Multipole Expansion Procedures

Theoretical Background.- As an alternative to a full solution of equations (24) to (26), a multipole expansion (MPE) procedure has been developed along the lines that we have found so useful in two dimensions (refs. 30 and 31). The MPE is based upon fundamental solutions of Laplace's equation and so there is no need to consider equations (22) to (26) directly. The procedure, to be described fully below, basically consists of fitting one component of the measured velocity data in a series expansion of the fundamental solutions. The coefficients of the series are then used to evaluate series expansions for the corresponding unconfined-flow distributions of the other two velocity components. We have found in our two-dimensional investigation that the MPE technique has several advantages.

The principal advantage of the MPE procedure is that the calculations are straightforward and the associated computer program is very efficient. In our two-dimensional numerical simulations (ref. 30) of a self-correcting wind tunnel, for example, the least-squares fit technique led to errors between the fit and the individual data points that were far smaller than any errors expected from experimental measurement inaccuracies. These simulations were carried out for two different airfoil-section shapes and for several values of the ratio of chord-to-control-surface-height. Furthermore, the MPE approach can be adapted readily, by means of alternative subroutines in the computer program, to any control-surface cross-sectional shape. Another advantage that we have found useful in our two-dimensional experiments (ref. 31) is that the MPE provides a straightforward analytic continuation from one control surface location to another. We have found it convenient in the two-dimensional experiments to measure each of the two velocity components at a different distance from the airfoil. The MPE handles this geometrical situation directly,

whereas an integral equation formulation, as in equations (24) or (25), would have to be generalized and solution would become more complicated. Finally, the MPE can be used, in conjunction with conventional wall-correction theory, to assess the accuracy of the flow about the model if the functional relationships are not satisfied exactly.

The MPE development has been carried out for linearized compressible flows. The Prandtl-Glauert equation has been assumed to be a valid approximation in the flow region external to the control surface. This formulation reduces to the incompressible flow case when $\beta = (1 - M_\infty^2)^{1/2}$ goes to one, where $M_\infty$ is the free-stream Mach number. The origin of the MPE will be assumed to coincide with the origin of the $x$, $y$, $z$ coordinate system in figure 1.

In a typical application of the self-correcting tunnel concept, either in a wind tunnel or in a numerical simulation of a tunnel, measurements of the disturbance velocity components, say $v_{x_m}$, $v_{n_m}$ and $v_{t_m}$ would be made at a number of locations on the control surface. For this discussion, we will consider all three components, although $v_{t_m}$ is really unnecessary as discussed above. The first step in the MPE technique is to fit either $v_{x_m}$ or $v_{n_m}$ by a series expansion in the appropriate component of fundamental singularity solutions of the Prandtl-Glauert equation. If $v_{x_m}$ is taken as the boundary condition on the external flow, a least-squares fit is carried out of the form

$$v_{x_m}(x, \theta) = \sum_{j=1}^{J} X_j \, \mathcal{V}_{x_j}(x, \theta; \beta) \tag{28}$$

where $\mathcal{V}_{x_j}$ is the velocity component induced in the $x$-direction by the $j^{th}$ singularity. Once the coefficients $X_j$ are found from the least-squares fit, the values of the other two components, $v_{n_c}[v_{x_m}]$ and $v_{t_c}[v_{x_m}]$, say, that correspond to $v_{x_m}$ if the flow is unconfined, can be evaluated by

$$v_{n_c}(x, \theta) = \sum_{j=1}^{J} X_j \, \mathcal{V}_{n_j}(x, \theta; \beta) \tag{29}$$

$$v_{t_c}(x,\theta) = \sum_{j=1}^{J} X_j \, \mathcal{V}_{t_j}(x,\theta;\beta) \tag{30}$$

where $\mathcal{V}_{n_j}$ and $\mathcal{V}_{t_j}$ are the velocity components induced in the $n$- and $t$-directions, respectively, by the $j^{th}$ singularity. These calculated values are then compared with the measured values $v_{n_m}$ and $v_{t_m}$. If they agree the flow is unconfined, but if they do not agree, the differences are a measure of the interference present.

Alternatively, $v_{n_m}$ can be fit in a series of the form

$$v_{n_m}(x,\theta) = \sum_{j=1}^{J} N_j \, \mathcal{V}_{n_j}(x,\theta;\beta) \tag{31}$$

whereupon $v_{x_c}[v_{n_m}]$ and $v_{t_c}[v_{n_m}]$ are given by

$$v_{x_c}(x,\theta) = \sum_{j=1}^{J} N_j \, \mathcal{V}_{x_j}(x,\theta;\beta) \tag{32}$$

$$v_{t_c}(x,\theta) = \sum_{j=1}^{J} N_j \, \mathcal{V}_{t_j}(x,\theta;\beta) \tag{33}$$

and $v_{x_c}$ and $v_{t_c}$ must be compared with $v_{x_m}$ and $v_{t_m}$, respectively.

The choice of functions in the MPE series is somewhat arbitrary. Any combination of point singularities or spatial distributions of singularities may be used, so long as they satisfy the Prandtl-Glauert equation, are linearly independent, and are fully contained within the control surface. We have developed two separate MPE methods, which will be discussed in turn. The first is based on point singularities and is called the original MPE, while the second, the modified MPE, is tailored specifically for wings.

Original MPE Method and Results.- In this MPE method, we followed our two-dimensional procedure to use a systematically defined set of point singularities that are generated from three of the basic singularities used in conventional wind-tunnel-wall correction analyses (ref. 40). These latter

singularities are the source, the velocity potential of which (called $\phi_1$ here for later convenience) is given by

$$\phi_1 = -\frac{1}{\left[x^2+\beta^2(y^2+z^2)\right]^{1/2}} \tag{34}$$

the so-called infinitesimal-span horseshoe vortex representing the component of the lift force in the $y$-direction, the potential of which ($\phi_{10}$, say) is given by

$$\phi_{10} = \frac{y}{(y^2+z^2)}\left\{1+\frac{x}{\left[x^2+\beta^2(y^2+z^2)\right]^{1/2}}\right\} \tag{35}$$

and the infinitesimal-span horseshoe vortex representing the $z$-component of the lift, the potential of which ($\phi_2$, say) is given by

$$\phi_2 = \frac{z}{(y^2+z^2)}\left\{1+\frac{x}{\left[x^2+\beta^2(y^2+z^2)\right]^{1/2}}\right\} \tag{36}$$

These three singularities can be derived by considering a source singularity ($\Phi_0$, say) which satisfies the Prandtl-Glauert equation for the acceleration potential $\Phi$, namely

$$\Phi_0 = -\frac{U_\infty}{\left[x^2+\beta^2(y^2+z^2)\right]^{1/2}} \tag{37}$$

If $\Phi_0$ is differentiated with respect to $x$ to find $\Phi_1$, which is then integrated according to the relationship which holds in steady flow between the acceleration potential and the velocity potential, namely

$$\phi(x,y,z) = \frac{1}{U_\infty}\int_{-\infty}^{x}\Phi(x',y,z)\,dx' \tag{38}$$

we obtain $\phi_1$. Similarly, differentiation of $\Phi_0$ with respect to $y$ and integration according to equation (38) yield $\phi_{10}$ while differentiation with respect to $z$ and the subsequent integration yield $\phi_2$.

The basic set of singularities that we have chosen, then, consists of the three singularities in equations (34) to (36) plus all of their linearly independent first and second derivatives. The resulting fifteen MPE singularities for general, nonsymmetrical flow cases are assumed to be located at the origin. They are presented in Table I as the velocity components $q_{x_j}$, $q_{y_j}$, and $q_{z_j}$, in the $x$-, $y$-and $z$-directions, respectively. The $y$- and $z$-components can be resolved into the $n$- and $t$-components $q_{n_j}$ and $q_{t_j}$ by reference to figure 1, namely

$$q_{n_j}(x, \theta; \beta) = -q_{y_j}(x, \theta; \beta) \sin \psi(\theta) + q_{z_j}(x, \theta; \beta) \cos \psi(\theta) \tag{39}$$

$$q_{t_j}(x, \theta; \beta) = -q_{y_j}(x, \theta; \beta) \cos \psi(\theta) - q_{z_j}(x, \theta; \beta) \sin \psi(\theta) \tag{40}$$

The terms in the series are arranged so that the first nine terms are those for flow configurations which are symmetrical about the $x$-$z$ plane; i.e., those for which $\phi_j$, $q_{x_j}$ and $q_{z_j}$ are even functions of $y$ and $q_{y_j}$ is an odd function of $y$. The remaining six terms extend the analysis to general three-dimensional configurations and are those for which $\phi_j$, $q_{x_j}$ and $q_{z_j}$ are odd functions of $y$ while $q_{y_j}$ is an even function of $y$. Therefore, symmetrical and general configurations are considered using $J$ = 9 and 15, respectively.

A computer program implementing the original MPE procedure has been written incorporating the subroutine for elliptical control-surface cross-sections. Preliminary checks of the program were carried out based on individual singularities and hand calculations. A more thorough checkout has been carried out using evaluations of the unconfined flow fields of typical wing and body representations. For wings, short computer programs have been written to evaluate the unconfined flow field at control surfaces enclosing wings with elliptical and constant spanwise loadings. A lifting-line representation consisting of finite-span horseshoe vortices has been constructed for this purpose following the guidelines of Hough (ref. 41). Another short program was written to evaluate the unconfined flow field at control surfaces enclosing Rankine solids (ref. 42), which are used to represent typical body shapes. The results for the unconfined-flow distributions of the axial and normal velocity components calculated with these programs are referred to as "exact" values in the discussion which follows, and are denoted by $v_{x_m}$ and $v_{n_m}$, respectively.

Both circular control-surface cross sections with $b/a$ = 1.0 and elliptical cross sections with $b/a$ = 0.5 have been examined in these check cases and the results generally are comparable. We will discuss here some typical results for symmetrical configurations in incompressible flow. The nine-term symmetrical MPE has been used to obtain these results, but a spot check with the general 15-term MPE shows that they are equivalent.

With the original program, wings with the ratios $b_w/a$ of span-to-control-surface-width of 0.25 and 0.5 were examined. The results are similar for both constant and elliptical spanwise loadings. For the larger ( $b_w/a$ = 0.5), elliptically-loaded wing with $b/a$ = 0.5, the axial and normal disturbance velocity components at the control surface, nondimensionalized in terms of $U_\infty$, the aspect ratio $AR$ and the lift coefficient $C_L$, are presented in figures 2 and 3, respectively, as functions of $\theta$ for two values of $x/a$. Since $v_{x_m}$ and $v_{n_m}$ are symmetrical about $\theta$ = 0, results in the cross-section plane of the lifting line ( $x/a$ = 0.0) are given on the right-hand sides of the figures, while results one half-width downstream ( $x/a$ = 1.0) are given on the left-hand sides. As can be seen from the figures, the MPE fits to $v_{x_m}$ and to $v_{n_m}$ are in considerable error and so lead to errors in the corresponding calculated distributions $v_{x_c}[v_{n_m}]$ and $v_{n_c}[v_{x_m}]$. In the case of the smaller wing ( $b_w/a$ = 0.25), on the other hand, the results are not presented because the MPE fits as well as the calculated distributions $v_{x_c}[v_{n_m}]$ and $v_{n_c}[v_{x_m}]$ are indistinguishable from the exact distributions to the scale of figures 2 and 3.

With the original program, Rankine solids with a diameter-to-length ratio $\tau$ of 0.2 also were considered at zero angle of attack for a circular control-surface cross section. Three different values of the ratio of body-length-to-control-surface-width $b_b/a$ were treated, namely 0.2, 0.5 and 1.0. For the smallest body ( $b_b/a$ = 0.2), the errors between $v_{x_m}$, $v_{n_m}$ and their MPE fits, and between $v_{x_m}$, $v_{n_m}$ and the calculated values $v_{x_c}[v_{n_m}]$ and $v_{n_c}[v_{x_m}]$, are very small, roughly comparable to the agreement for wings with $b_w/a$ = 0.25. For the body with $b_b/a$ = 0.5, the errors are significantly larger, roughly of the same magnitude as for the wings with $b_w/a$ = 0.5 in figures 2 and 3. The results for the axial and normal disturbance velocities, nondimensionalized by

$U_\infty$, of the largest body ( $b_b/a$ = 1.0) are presented in figures 4 and 5, respectively, as a function of $x/a$ for $\theta$ = 0. Although the exact values of $v_{x_m}$ and $v_{n_m}$ are axisymmetric, the least-squares fits in the MPE deviate somewhat from axisymmetry because of the influence of the higher-order terms in the MPE series. However, the $\theta$ = 0 values presented are indicative of the errors which exist for this case at all $\theta$ .

The original form of the MPE procedure based on point singularities verifies that the exact unconfined-flow velocities induced by typical wing configurations satisfy the functional relationships for wings with $b_w/a$ = 0.25. However, the original form of the MPE does not verify unconfined flow for wings with $b_w/a$ = 0.5. Moreover, although it verifies unconfined flow for a Rankine solid with $\tau$ = 0.2 and $b_b/a$ = 0.2, it does not for longer bodies with $b_b/a$ = 0.5 and especially with $b_b/a$ = 1.0. These inaccuracies were unexpected because of the success of the two-dimensional MPE, which is based on point singularities, for different airfoil sections and various ratios of chord-to-control-surface-height.

An understanding of the full significance of this failure to verify unconfined flow in figures 2 to 5 by the original MPE requires an estimate of the implications of these errors on the flow about the model itself. This is the question addressed in the later section on accuracy assessment. Results which are developed there show that the magnitudes of the errors in figures 2 to 5, which are inherent in the original MPE, are not indicative of the errors incurred at the model. For example, the errors implied in the pressure distribution on the Rankine solid by the inaccurate fits of figures 4 and 5 are only about three percent as will be shown. The accuracy-assessment method to be described below is directly applicable only to control surfaces with a circular cross section. Nevertheless, for the elliptical control-surface cross section used for the wing case in figures 2 and 3, we estimate that the error in lift coefficient is less than one percent for a wing with an aspect ratio of one and considerably less than one-half percent for wings with aspect ratios of five or more.

Modified MPE Method and Results.- Although the accuracy-assessment results indicate that the errors in the flow about the model are not as large as the errors in the original MPE fits themselves, it is still important to eliminate these inherent errors as far as possible. Consequently, a modified form of the MPE analysis has been developed in order to extend the size of the wings ($b_w/a$) which can be treated with high accuracy. No attention has been given to extending the range of body lengths ($b_b/a$) which can be treated accurately although the same principles should be applicable in that case as well.

The modified MPE has been carried out for symmetrical configurations only; i.e., $J = 9$ is considered as the limit in the MPE. As mentioned earlier, the choice of singularities in the MPE is somewhat arbitrary. Therefore, in order to extend the MPE technique to larger $b_w/a$ values, we have replaced the infinitesimal-span horseshoe vortex with lift in the $z$-direction (i.e., term 2 in Table I) by a finite-span horseshoe vortex similarly oriented. The semi-span $b_v$ of the horseshoe vortex is arbitrary, but for all examples to date, we have chosen $b_v = \sqrt{3}\, b_w/2$. This value matches exactly (ref. 43) the first two terms in a multipole expansion of the velocity potential for an elliptically-loaded lifting-line representation of a wing. The strength $\Gamma_v$ of the horseshoe vortex is given by

$$\Gamma_v = U_\infty C_L b_w^2 / AR\, b_v \tag{41}$$

The check cases for the modified MPE computer program have all considered the unconfined flow about elliptically-loaded wings located within an elliptical control surface with $b/a = 0.5$. The first example is for $b_w/a = 0.5$; i.e., the case treated by the original MPE and presented in figures 2 and 3. The fit and calculated values using the modified form of the MPE are indistinguishable from the exact distributions in figures 2 and 3 so are not presented there explicitly. The modified MPE thus verifies very accurately that this flow field is unconfined and so represents a significant improvement over the original form.

Additional cases were run for $b_w/a = 0.75$ and 0.875 using the modified MPE. The agreement in the former case is satisfactory, but for the latter the agreement is not, particularly for $v_n$, as shown in figures 6 and 7. An additional measure of the errors involved is presented in Table II, which gives the rms errors between the exact, unconfined-flow values $v_{x_m}$ and $v_{n_m}$ (as normalized) and the fits to them, as well as the rms errors between the exact values and the calculated values $v_{x_c}[v_{n_m}]$ and $v_{n_c}[v_{x_m}]$. Also, the comparison is given in Table II between the exact values of the tangential velocity $v_{t_m}$ and the values $v_{t_c}[v_{x_m}]$ and $v_{t_c}[v_{n_m}]$ as calculated from the fits to $v_{x_m}$ and $v_{n_m}$, respectively. There are no fits to $v_{t_m}$ as discussed above. Also included in Table II are the errors for $b_w/a = 0.5$ with the original MPE method. Although we can make only rough estimates on the basis of our accuracy-assessment method, the errors indicated at the model, even for $b_w/a = 0.875$, are still small, probably less than one percent for aspect ratios of one or greater.

We conclude from the cases presented here that the modified MPE is a distinct improvement over the original form and for $b/a = 0.5$ should be applicable up to $b_w/a = 0.75$ with reasonable accuracy. Beyond this value, the details of the wing loading distribution become more important to the induced velocity distributions at the control surface so that the MPE terms that we have included do not verify accurately that the flow is unconfined.

A single example has been carried out for compressible, subcritical flow to examine the capability of the modified MPE program in this flow regime. The case considered was $b/a = 0.5$, $b_w/a = 0.5$ and $M_\infty = 0.6$. The results are comparable to the incompressible-flow results for the same geometry.

Additional exploration of the utility of the modified MPE program was carried out by offsetting the wing from the origin of the control-surface coordinate system. The MPE singularities remained at the control-surface origin. In this way, we could examine the applicability of the MPE in its present form to configurations with multiple lifting surfaces, e.g., wing-tail combinations. For a wing with $b_w/a = 0.5$ and an elliptical control surface

with $b/a$ = 0.5, we ran several examples including one with the wing offset in the $x$-direction by $x_o/a$ = 0.25 (figures 8 and 9) and one with the wing offset in the $z$-direction by $z_o/a$ = 0.25 (figures 10 and 11). It is obvious from these figures that neither the least-squares fits nor the subsequent calculations of $v_{z_c}\,[v_{n_m}]$ and $v_{n_c}\,[v_{x_m}]$ are satisfactory. Therefore, the modified MPE program does not verify that these flows are unconfined.

These same examples have been rerun with the origin of the MPE moved to coincide with the origin of the wing. For the $x_o/a$ = 0.25 offset, excellent agreement was obtained since the translation of the origin reduced this example to exactly that of figures 2 and 3. For the $z_o/a$ = 0.25 offset, however, the agreement still is not satisfactory, being roughly comparable to that shown in figures 6 and 7 for $b_w/a$ = 0.875. This follows because the translation of the wing has brought the wing tips nearer to the control surface (as shown in the sketches on figures 10 and 11). Therefore, the details of the wing loading distribution again have become so important that we have not included enough MPE terms to verify with confidence that the flow is unconfined.

Modified MPE with Ground Effect.- The effect of the ground on a model in a wind tunnel can be included readily in the MPE analysis of the external-flow functional relationships. The boundary condition that there can be no normal flow through the ground plane must be satisfied as well as the condition that the disturbances must vanish away from the model and its wake in the other directions. The method of images can be applied to insure that the normal velocity component vanishes at the ground plane. Within the framework of the MPE technique, this requires that we must add to each basic MPE term its image term.

The modified MPE computer program for symmetrical flows has been extended so that evaluation of the external-flow functional relationships in ground effect may be carried out. The extension is straightforward in terms of the use of image singularities to the basic singularities in Table I. In particular, for zero normal flow velocity at a ground plane located a distance $h_q$ below the model, images must be located at a distance $2h_q$ below the model.

The images of those singularities in Table I which have expressions for $v_z$ that are odd in $z$ (terms 1, 3, 5, 6, 8, 10, 11, 13 and 15) have the same strength and sign as the basic singularities. The images of those singularities with expressions for $v_z$ that are even in $z$ (terms 2, 4, 7, 9, 12 and 14) have the same strength, but are of opposite sign. The finite-span horseshoe vortex which replaces term 2 also is even in $z$ . The symmetrical program has been rewritten so that a single program handles flows both in and out of ground effect depending upon the form of the input.

We have carried out a few numerical examples to check the program for wings in ground effect. Input data for the control-surface velocities in these cases have been found by adding the appropriate images to the lifting-line representation of the wing. Results for a wing located 0.8 semispans (or 0.4 spans) above the ground with $b/a = 0.5$, $b_w/a = 0.75$ and so $h_g/a = 0.6$ are given in the usual format in figures 12 and 13. The errors in the fits and calculated values in this case are comparable in magnitude to those found for a wing of the same span in fully unconfined flow, see Table II. We conclude that the ground-effect option in the modified MPE program is working satisfactorily.

Discussion of MPE Results.- The MPE procedures and the computer programs which implement them provide a means for rapid evaluation of the unconfined-flow functional relationships both in and out of ground effect. In its original form with point singularities, the MPE is limited in its exact satisfaction of the functional relationships to wings with ratios of span-to-control-surface-width $b_w/a$ of less than 0.5 for control-surface cross sections that are both circular ( $b/a = 1.0$) and elliptical with $b/a = 0.5$. It is also limited to bodies with ratios of length-to-control-surface-width $b_b/a$ of less than 0.5 for circular control-surface cross sections. It has been shown that an extended range of validity can be achieved in the modified form of the MPE by a more accurate representation of the wing with a finite-span horseshoe vortex replacing the corresponding point singularity. However, the accuracy-assessment method described in a later section reveals that even the apparently large errors in satisfaction of the functional relationships by these MPE methods lead to relatively small errors in the flow about the body.

Thus, we conclude that the form of the MPE should be tailored to the specific model being tested for most accurate evaluation of the unconfined-flow functional relationships in an experimental situation. This is contrary to our two-dimensional experience where a single MPE based on point singularities had broad applicability in theoretical studies. However, recent experience in our two-dimensional experiments has revealed another weakness of the MPE. In particular, it appears that the errors between the least-squares fit and the measured data points are no longer negligible in experimental iterations toward unconfined flow. If this is the case, these errors will reduce the accuracy of the entire self-correcting wind tunnel system. A more thorough assessment of the implications of these errors is underway in two dimensions.

Consequently, we believe that a more general, less configuration-tailored method for evaluating the functional relationships is desirable. This is necessary especially when large deformations of the trailing vortex system occur and definitely will be required in extension of the analysis to include the propulsion-system efflux when it exits through the control surface into the external flow in the vicinity of the model. The development of a singularity distribution method, such as a source distribution or vortex lattice procedure would provide such a general method for evaluating the functional relationships. To this end, development of a source distribution method was begun and is described next.

## Source Distribution Method

Development of a source distribution method along the lines of Hess and Smith (refs. 37-39) has begun as an alternative to the MPE procedures. This method will complement the MPE and will provide a more general method for evaluating the unconfined-flow functional relationships. The source distribution method has been carried out for symmetrical flow fields within an elliptical control-surface cross section in incompressible flow. Initially, the method evaluates $v_{x_c}[v_{n_m}]$ and $v_{t_c}[v_{n_m}]$ with $v_{n_m}$ prescribed as the

boundary condition on the control surface for nonlifting bodies. Generalizations to $v_{x_m}$ as the boundary condition, to lifting bodies, and to compressible flow would be the next steps in the development.

The computer program implementing the source distribution method is a straightforward application of references 37-39 to a control surface with elliptical cross section. The principal difference concerns the normal flow boundary condition which is no longer dependent on the control surface shape, but rather is a set of normal velocity measurements. In the program, the normal velocity component $v_{n_m}$ is read in over a range of $\theta$ values for each of several different $x$ values. A cubic spline interpolation procedure is used, first in $\theta$ at a constant $x$, and then in $x$ at constant $\theta$, to obtain $v_{n_m}$ at the centroid of each elemental source panel. These interpolated values are then the boundary conditions for determining the elemental source strengths. Similar interpolations are made in $v_{x_m}$ and $v_{t_m}$ to facilitate their comparison with $v_{x_c}[v_{n_m}]$ and $v_{t_c}[v_{n_m}]$. A direct solution of the resulting set of linear algebraic equations is used to determine the source strengths, whereupon the desired output quantities, e.g., $v_{x_c}[v_{n_m}]$ and $v_{t_c}[v_{n_m}]$, are evaluated.

The initial form of the program has been completed, checked and a trial case has been run. This case is the flow about the same Rankine solid with $\tau = 0.2$ and $b_b/a = 0.2$ that was described earlier. The control surface is assumed to have a circular cross section with $b/a = 1.0$. For this first trial case, a coarse breakdown has been used with 96 source panels representing one half of the symmetrical control surface. These 96 panels consist of six equally-spaced $\theta$ increments at each of sixteen non-equally-spaced $x$ increments. In figure 14, the resulting axial velocity component distribution $v_{x_c}[v_{n_m}]$, nondimensionalized by $U_\infty$, is plotted as a function of $x/a$ for $\theta = 0°$. This distribution is compared with the exact distribution $v_{x_m}$ as well as with $v_{x_c}[v_{n_m}]$ as evaluated by the original form of the MPE. The flow is fully-axisymmetric, giving the same values as in figure 14 at all values of $\theta$. In addition, $v_{t_c}[v_{n_m}]$ is zero as it should be. We conclude from this example that even with a coarse breakdown, the source method shows considerable promise.

The source distribution program can be made very efficient for routine usage after all the required generalizations are made. Once the source panel geometry is decided upon for a given control-surface cross section ($b/a$), the matrix of the normal velocity induction can be set up and inverted once and for all (assuming that the inversion can be carried out accurately) and stored on tape. Then each time the functional relationships for unconfined flow must be evaluated, it would be a matter only of reading in and interpolating in the $v_{x_m}$, $v_{n_m}$ and $v_{t_m}$ data, of evaluating the source strengths from the measured $v_{n_m}$ by use of the inverse matrix, and then evaluating $v_{x_c}$ $[v_{n_m}]$ and $v_{t_c}$ $[v_{n_m}]$. Therefore, the source distribution method is also potentially an efficient method for verifying that a given wind tunnel flow is unconfined.

## APPLICATION OF FUNCTIONAL RELATIONSHIPS TO ASSESSMENT OF WIND-TUNNEL INTERFERENCE

### General

The question naturally arises as to how accurately the unconfined-flow functional relationships must be satisfied for the flow about the model to be interference free in a practical sense. This becomes of paramount importance in application of the concept to testing in existing conventional wind tunnels. For answers to this question, the flow within the tunnel must be considered as well as the flow exterior to the control surface.

This requires that the flow within the tunnel be modeled theoretically. Obviously, the more accurate the representation of this internal flow, the better the accuracy question can be answered. Thus, for the type of wind tunnel models considered in the previous section, a singularity distribution representation would be desirable. However, a first estimate of the inaccuracy involved in failure to satisfy exactly the unconfined-flow functional relationships can be found by the simplified method described below. Before presenting this method, it should be remarked that the accuracy question must be

addressed ultimately experimentally. We have found this to be the case in our two-dimensional transonic self-correcting wind tunnel (ref. 31).

## MPE-Based Accuracy-Assessment Model

Development of Method.- The most direct way of treating this question theoretically is to consider a generalization of conventional wall-correction theory, as presented in reference 40, for example, using the original form of the MPE technique. The linearized disturbance velocity potential $\phi$ for the interior flow within the tunnel is assumed to satisfy the Prandtl-Glauert equation as written in the appropriate coordinate system. In contrast to conventional wall-correction theory, however, the theoretical wall characteristics, e.g., those for a solid wall, open jet, perforated wall or slotted wall, are replaced by the disturbance velocity components, $v_{x_m}$ and $v_{n_m}$, that are measured along the control surface $\mathcal{S}$. Then the boundary condition at $\mathcal{S}$, so far as the interior flow is concerned, is either

$$\partial \phi / \partial x \Big]_{\mathcal{S}} = v_{x_m} \tag{42}$$

or

$$\partial \phi / \partial n \Big]_{\mathcal{S}} = v_{n_m} \tag{43}$$

We note that either equation (42) or equation (43) can be specified as a boundary condition on the interior flow, but not both. Prescribing both would overspecify the problem and so make it improperly posed. In the subsequent discussion, we will consider equations (42) and (43) as alternative boundary conditions on the interior flow. It is assumed further, just as in conventional theory, that $\phi$ can be written as

$$\phi = \bar{\phi} + \phi^* \tag{44}$$

where $\bar{\phi}$ is the idealized potential of the model in unconfined flow and $\phi^*$ is the interference potential introduced by the tunnel boundaries. Since the

idealized potential $\bar{\phi}$ is assumed to satisfy the Prandtl-Glauert equation, $\phi^*$ also must satisfy it.

The analysis will be carried through first for the $v_{x_m}$ boundary condition, equation (42), which becomes, using equation (44),

$$\partial \phi^* / \partial x \Big]_S = v_{x_m} - \partial \bar{\phi} / \partial x \Big]_S \tag{45}$$

At this point, we continue to follow conventional correction theory by expressing $\bar{\phi}$ in terms of the basic singularities of reference 40. This is equivalent in our MPE terminology, to writing

$$\partial \bar{\phi} / \partial x \Big]_S = \sum_{j=1}^{J} C_j \, v_{x_j} \tag{46}$$

where the coefficients $C_j$ are determined by geometrical and measured characteristics of the model being tested. For example, the terms for $J = 3$ generally (ref. 40) are considered for symmetrical configurations and are, respectively; the source whose strength is proportional to the measured drag (wake blockage), namely

$$C_1 = \frac{U_\infty C_D S_\omega}{8\pi} \tag{47}$$

where $C_D$ is the drag coefficient and $S_\omega$ is the reference area of the model; the $z$-directed infinitesimal-span horseshoe vortex, whose strength is proportional to the measured lift (lift interference), namely

$$C_2 = \frac{U_\infty C_L S_\omega \beta}{8\pi} \tag{48}$$

and the upstream-directed doublet, whose strength is proportional to the model volume $V$ (solid blockage), namely

$$C_3 = \frac{U_\infty V}{4\pi} \tag{49}$$

In our generalization of classical correction theory, we also expand $v_{x_m}$ in the MPE fit by equation (28). Then combining equations (28), (45) and (46), we have as the boundary condition on the interference potential.

$$\partial \phi^* / \partial x \Big]_S = \sum_{j=1}^{J} (X_j - C_j) \gamma_{x_j} \tag{50}$$

We note at this point that the conventional open-jet boundary condition, namely $\partial \phi / \partial x \Big]_S = 0$, is the same as equation (42) with $v_{x_m} = 0$, so that $\phi^*$ for an open jet would satisfy equation (50) with $X_j = 0$ for all $j$.

The correction procedure thus would proceed as follows. The experiment would be run and all appropriate quantities would be measured, both on the model ( $C_L$ , $C_D$ ) and at the control surface ( $v_{x_m}$). From the measured data, the $X_j$ and $C_j$ would be determined. Then results of conventional open-jet correction theory would be used directly to determine interference velocities at the model, with $C_j$ replaced by $C_j - X_j$.

Alternatively, if $v_{n_m}$ is measured at $S$ instead of $v_{x_m}$, a similar analysis can be carried out. In this case, the $v_{n_m}$ boundary condition, equation (43), becomes

$$\partial \phi^* / \partial n \Big]_S = v_{n_m} - \partial \bar{\phi} / \partial n \Big]_S \tag{51}$$

We again express $\bar{\phi}$ in terms of conventional correction theory, namely

$$\partial \bar{\phi} / \partial n \Big]_S = \sum_{j=1}^{J} C_j \gamma_{n_j} \tag{52}$$

where the $C_j$ are still given in equations (47) to (49) for $J = 3$. The MPE expansion fit in equation (31) then can be combined with equations (51) and (52) to give

$$\partial \phi^* / \partial n \Big]_S = \sum_{j=1}^{J} (N_j - C_j) \gamma_{n_j} \tag{53}$$

The conventional solid-wall boundary condition, namely $\partial\phi/\partial n\big]_S = 0$, is the same as equation (43) with $v_{n_m} = 0$, so that $\phi^*$ for a solid wall would satisfy equation (53) with $N_j = 0$ for all $j$. Therefore, the results of conventional solid-wall correction theory would be used directly to determine interference velocities at the model, with $C_j$ replaced by $C_j - N_j$.

In this procedure, therefore, corrections would be made on the basis of conventional interference theory and the MPE fit to the measured velocities at the control surface. We can see immediately that if the flow is actually unconfined, $X_j = N_j \cong C_j$ and the corrections would be zero. The approximate equality here reflects the fact that the $C_j$ are based on an idealized representation of the model whereas $v_{x_m}$ and $v_{n_m}$ are measured as the actual disturbances introduced by the model.

For tunnels with circular and rectangular cross sections, the results for $J = 3$ are available in the literature. In particular, using the $v_{x_m}$ boundary condition for circular cross sections, the interference velocity components $\Delta_x v_x$ and $\Delta_x v_3$, say, evaluated at the origin, and their longitudinal gradients $\Delta_x(\partial v_x/\partial x)$ and $\Delta_x(\partial v_3/\partial x)$, also evaluated at the origin, are

$$\Delta_x v_x = -0.41 \frac{(C_3 - X_3)}{\beta^3 a^3} \tag{54}$$

$$\Delta_x(\partial v_x/\partial x) = -0.41 \frac{(C_1 - X_1)}{\beta^3 a^3} \tag{55}$$

$$\Delta_x v_3 = -\frac{(C_2 - X_2)}{\beta a^2} \tag{56}$$

$$\Delta_x(\partial v_3/\partial x) = -0.80 \frac{(C_2 - X_2)}{\beta^2 a^3} \tag{57}$$

Similarly if the $v_{n_m}$ boundary condition is used to estimate the errors, the results for a circular control-surface cross section are

$$\Delta_n v_x = 2 \frac{(C_1 - N_1)}{\beta^2 a^2} + 1.53 \frac{(C_3 - N_3)}{\beta^3 a^3} \tag{58}$$

$$\Delta_n (\partial v_x / \partial x) = 1.53 \frac{(C_1 - N_1)}{\beta^3 a^3} \tag{59}$$

$$\Delta_n v_z = \frac{(C_2 - N_2)}{\beta a^2} \tag{60}$$

$$\Delta_n (\partial v_z / \partial x) = \frac{(C_2 - N_2)}{\beta^2 a^3} \tag{61}$$

Extension of this accuracy-assessment procedure to include the $j \geq 4$ terms could be carried out in a similar way to the analysis of reference 40 and the references given therein. In such an analysis for circular cross sections, the solutions are found in terms of Fourier integrals containing Bessel functions. Similar results are not available for elliptical cross sections for any $j$, but could be found in an analogous fashion. Unfortunately, the solutions would be in terms of Mathieu functions (ref. 44), which would be unwieldy for practical computation. Results are available (ref. 40) for rectangular cross sections for $J = 3$ and the present procedures could be adapted to that case. None of these further extensions and adaptations have been carried out, however, Instead, the existing analysis has been applied to the examples of the earlier sections to show the errors inherent in failure of the original MPE to satisfy the unconfined-flow functional relationships exactly for circular control-surface cross sections.

Application to Wings.- The MPE-based accuracy-assessment method has been applied to several wings, as represented by elliptically-loaded lifting lines. The unconfined-flow perturbation velocity distributions were computed at a control surface with a circular cross section ( $b/a = 1.0$) as described earlier and the original form of the MPE was used. In the application of the MPE for these symmetrical flow fields, nine terms were retained in the MPE, but as described above, the accuracy estimates are based on the coefficients of the first three terms.

In this lifting-line representation of the wings, $C_1$ and $C_3$ are zero identically and from the MPE fit to the data, $X_1$, $X_3$, $N_1$ and $N_3$ have been calculated to be zero. Therefore, the interference velocity components induced at the origin (midspan of the lifting line) are, from equations (54) to (61), the upwash $\Delta v_z$ and its gradient in the $x$-direction $\Delta(\partial v_z/\partial x)$. For elliptically-loaded, flat, untwisted wings with an ideal lift-curve slope of $2\pi$, the lift coefficient is given by (ref. 45)

$$C_L = \frac{2\pi AR\,\alpha}{2 + \beta AR} \tag{62}$$

Alternatively, from equation (48), we have

$$C_L = \frac{2\pi AR\,C_2}{U_\infty b_w^2 \beta} \tag{63}$$

where the definition of the aspect ratio has been used. The expressions for the $z$-component of the interference velocity can be related to an angle of attack error $\Delta\alpha$, and an effective angle of attack error $\Delta\alpha_o$ due to a parabolic-arc camber effect, by

$$\Delta_x\alpha = \frac{\Delta_x v_z}{U_\infty} = -\frac{(C_2 - X_2)}{U_\infty \beta a^2} \tag{64}$$

$$\Delta_x\alpha_o = \frac{b_w}{2U_\infty AR}\,\Delta_x(\partial v_z/\partial x) = -\frac{2b_w(C_2 - X_2)}{5U_\infty \beta^2 a^3 AR} \tag{65}$$

for the $v_{x_m}$ boundary condition, and by

$$\Delta_n\alpha = \frac{\Delta_n v_z}{U_\infty} = \frac{(C_2 - N_2)}{U_\infty \beta a^2} \tag{66}$$

$$\Delta_n\alpha_o = \frac{b_w}{2U_\infty AR}\,\Delta_n(\partial v_z/\partial x) = \frac{b_w(C_2 - N_2)}{2U_\infty \beta^2 a^3 AR} \tag{67}$$

for the $v_{n_m}$ boundary condition. If $\Delta\alpha$ and $\Delta\alpha_o$ are positive, they imply that the effective angle of attack of the model in the tunnel is larger than the geometric angle of attack. Thus a negative increment in $C_L$ is required

to interpret the measured data correctly. This increment is given by equation (62) as

$$\Delta C_L = - \frac{2\pi AR \Delta(\alpha + \alpha_o)}{2 + \beta AR} \tag{68}$$

Combining equations (63) to (68), we obtain expressions for the errors based on $v_{x_m}$ and $v_{n_m}$, respectively, as

$$\frac{\Delta_x C_L}{C_L} = \frac{(b_w/a)^2 \left[1 + \frac{2(b_w/a)}{5\beta AR}\right]\left(1 - \frac{X_2}{C_2}\right)}{2 + \beta AR} \tag{69}$$

$$\frac{\Delta_n C_L}{C_L} = - \frac{(b_w/a)^2 \left[1 + \frac{(b_w/a)}{2\beta AR}\right]\left(1 - \frac{N_2}{C_2}\right)}{2 + \beta AR} \tag{70}$$

The errors that are implied in the lift coefficient by failure of the original MPE to satisfy the functional relationships exactly have been evaluated by equations (69) and (70) for some incompressible flow cases. They are the errors inherent in the original form of the MPE for a given $b_w/a$. The wings treated have aspect ratios $AR$ of 1, 5 and 10 and ratios of span-to-control-surface-width $b_w/a$ of 0.2, 0.4, 0.6 and 0.8. The results are presented in Table III. As can be seen, the errors are less than 1% in all cases. Also, there is a difference in sign as well as magnitude between the errors based on $v_{x_m}$ and those based on $v_{n_m}$. This provides an additional indication of the errors inherent in the original form of the MPE. Overall, the errors are so small that the effect at the model is negligible and so the inherent failure to satisfy the functional relationships exactly using the MPE is not important for the geometrical range considered.

The advantages offered by the self-correcting wind tunnel can be seen quantitatively as follows. For the most severe geometry in Table III, namely $AR = 1$ and $b_w/a = 0.8$, the error in a solid-wall wind tunnel of circular cross section would be $\Delta_n C_L / C_L = -0.299$; i.e., an error of about thirty percent. If the walls of the tunnel can be adjusted so that the $v_{n_m}$ distribution

is within ±10% of the unconfined-flow values, then $(1-\frac{X_2}{C_2})$ will be approximately ±0.1 and so $\Delta_n C_L / C_L$ will be only about ±0.03; i.e., about three percent.

Application to Bodies.- The MPE-based accuracy-assessment method also has been applied to several axisymmetric bodies at zero angle of attack as represented by Rankine solids of diameter-to-length ratio $\tau$ of 0.2. The unconfined-flow distributions were computed at a control surface with a circular cross section ( $b/a = 1.0$) as described earlier and the original form of the MPE was used. As for the wings, nine terms in the MPE were used and the accuracy estimates were based on the first three.

For the Rankine solids, $C_1$ and $C_2$ are zero identically and from the MPE fit to the data, $X_1$ , $X_2$ , $N_1$ and $N_2$ have been calculated to be zero. Moreover, since the gradients of the axial velocity in the $\chi$-direction are independent of $C_3$ , $X_3$ and $N_3$ , then the only nonzero interference velocity components induced at the origin (center of the body) from equations (54) to (61) are the axial components $\Delta v_\chi$ . If $\Delta v_\chi$ is positive, it implies that the effective axial velocity at the model is larger than the freestream velocity. Consequently, a negative increment in pressure coefficient $C_p$ is required to interpret the measured data correctly. This increment is related to $\Delta v_\chi$ by

$$\frac{\Delta C_p}{C_p} = \frac{1}{\left[1 + \Delta(v_\chi / U_\infty)\right]^2} - 1 \tag{71}$$

which becomes, neglecting higher-order terms,

$$\frac{\Delta C_p}{C_p} = -2\,\Delta(v_\chi / U_\infty) \tag{72}$$

For Rankine solids, the volume is given by

$$\mathcal{V} = 2\pi b_b^3 T^2 \tag{73}$$

where $T$ is a function of the diameter-to-length ratio $\tau$ given implicitly by $T = \tau\,(1 + \tau^2 - T)^{1/4}$. Combining equations (49), (54), (58), (72) and (73) gives

$$\frac{\Delta_x C_p}{C_p} = \frac{0.41\,(b_b/a)^3\,T^2\left(1-\frac{X_3}{C_3}\right)}{\beta^3} \tag{74}$$

$$\frac{\Delta_n C_p}{C_p} = -\frac{1.53\,(b_b/a)^3\,T^2\left(1-\frac{N_3}{C_3}\right)}{\beta^3} \tag{75}$$

The errors that are implied in the pressure coefficients on a Rankine solid by the inherent failure of the original MPE to satisfy the unconfined-flow functional relationships exactly have been evaluated using equations (74) and (75). The Rankine solids considered have $\tau = 0.2$ (and so $T = 0.191928$) and lengths $b_b/a = 0.2$, 0.5 and 1.0. The results for incompressible flow are given in Table IV. The errors here are larger than they are for the wing cases in the previous section, reaching nearly three percent for $b_b/a = 1.0$. There is a difference in sign as well as magnitude here, too. Nevertheless, the effect of the inherent failure of the MPE to satisfy the unconfined-flow functional relationships exactly has a relatively small effect except for the largest body size considered here. Clearly, a modified MPE for treating bodies of this size could be developed, as was the modified MPE for treating wings.

## Improved Methods

The simplified method based on the original MPE and classical correction theory has proved useful in assessing the accuracy of the flow about the model for control surfaces with circular cross sections. As seen from the examples, however, the inaccuracies in the MPE fit sometimes give indicated errors of opposite signs depending on whether the axial or normal component of the disturbance velocity is used as the boundary condition. Thus, the method seems best suited only for making rough estimates of the errors introduced by wall interference but is not suitable for actual data correction purposes. Extension to other cross-section shapes could be made and it also might be possible to extend the analysis to make use of the modified MPE where the point singularity representing the lift is replaced by a horseshoe vortex of finite span.

The real requirement for assessing the accuracy in the flows about models, however, is for a better representation of the interior flow within the test section. This need could be served best, probably, by combining a lifting-surface representation of wing-fuselage models with a source distribution method of representing the control surface. The source distribution method developed above for evaluating the functional relationships in the exterior flow could be adapted for use in the interior flow. Such a model would provide more accurate assessments of the errors at models when the functional relationships are not satisfied exactly. Moreover, the assessments could be used further to provide corrections to the data. In this way, the measured values of the disturbance velocity components at the control surface would be used as the boundary conditions on the interior flow instead of assumed wall characteristics. Use of measured data is especially important for ventilated test sections because it has been shown recently by several investigators, for example Vidal and Rae (ref. 46), that the conventional wall boundary conditions for these test sections (as used in reference 40, for example) are not representative of the actual wall behavior. Therefore, use of the measurements with an accurate interior flow representation could eliminate the present uncertainty in calculating wall-interference corrections, especially in ventilated test sections.

## CONCLUDING REMARKS

This study on the application of the adaptive-wall, or self-correcting, wind tunnel concept to testing in fully subsonic, three-dimensional flows has led to the following concluding remarks.

1. The control surface at which flow disturbances are measured generally should have a height-to-width ratio less than one for greatest applicability both in and out of ground effect. Elliptical and rectangular shapes are suitable choices for the control-surface cross section, which need not have the same shape as that of the tunnel. Formulation of the unconfined-flow

functional relationships shows that the axial disturbance velocity component and the component normal to the control surface are sufficient for the redundant measurements. The remaining orthogonal component tangential to the control surface cannot be used because it is not independent of the axial component.

2. The original multipole expansion (MPE) procedure based on point singularities in three dimensions does not evaluate the functional relationships accurately over as wide a range of model-to-control-surface-size as does its two-dimensional counterpart. Modifications to the MPE by replacing selected point singularities with singularity distributions can tailor the MPE procedure to particular model configurations. For wings, the modified MPE developed here is accurate over a significantly larger range of span-to-control-surface-width. A different approach based on a distribution of source panels representing the control surface offers promise of an accurate, efficient, and less configuration-oriented way of evaluating the functional relationships.

3. A procedure for estimating the interference at the model when the functional relationships are not satisfied exactly has been developed for circular control surfaces. It uses the disturbance velocity measurements, the MPE evaluation and classical wall-correction theory. Applications of this procedure show that for a given magnitude of error in satisfaction of the functional relationships, the magnitude of the interference at the model is much less. Therefore, achievement of a given accuracy in the approach to interference-free flow at the model imposes a less severe requirement on the accuracy in the satisfaction of the functional relationships.

4. Development of a suitable representation of the propulsion-system efflux outside the control surface is the next important step required to apply the concept to V/STOL testing. Development of more accurate simulations of the flow within the control surface is a necessary step for applications to existing tunnels. These simulations would permit development of improved

correction procedures, especially for ventilated tunnels for which the wall boundary conditions are not well founded. Finally, development of experimental procedures, particularly the measurement techniques, should be carried out for use in both existing and future tunnels.

# APPENDIX

## THE CONCEPT OF A SELF-CORRECTING WIND TUNNEL

### Unconfined Flow

An ideal to strive toward would be a V/STOL tunnel that would always adjust itself to eliminate the constraining effects of its boundaries, for any configuration tested at any angle of attack and/or sideslip, for any deflection angle of the propulsion-system efflux, and at any flight speed from hover through transition to cruise. This ideal tunnel could be approached if it were possible to sense departures from unconfined-flow conditions in the working section and to modify the tunnel geometry accordingly, until the readings of appropriate sensors confirm that an unconfined-flow pattern exists in the working section, whereupon test data would be read and recorded. It seems clear that this could be done, in principle, by changing the shape of the tunnel boundary, for unconfined-flow conditions could always be achieved by adjusting the walls to the configuration of the stream surfaces of unconfined flow past the given model. Another possibility would be to change the effective shape of the tunnel boundary by appropriate distributions of tunnel-wall porosity and plenum pressure behind the walls. In either case, the possibility of providing active control of the flow by wall adjustments leads us to the concept of a self-correcting, or adaptive-wall, wind tunnel (ref. 29).

The essential basis of the scheme envisioned is that unconfined-flow conditions in the working section can be determined by means of the readings of suitably placed sensors within the airstream. Let figure 15(a) represent a V/STOL configuration in an unbounded stream of given velocity $U_\infty$. Let the space surrounding this vehicle consist of an interior region, I, and an exterior region, II, where the boundary $S$ between I and II is an imaginary one, located near the proposed wind-tunnel boundary but having no effect on

the flow.* The presence of the model, including the propulsion-system efflux, produces disturbances of the uniform stream; let the values of the disturbance velocity components, pressure, ... at $\mathcal{S}$ be $v_x$ , $v_y$ , $v_z$ , $p$ ... If the flow field outside $\mathcal{S}$ , i.e., in II, is considered by itself, see figure 15(b), specification of these values of velocity, pressure and density, including those characterizing the mass- and momentum-flow rates of the efflux, constitutes, along with the equations of motion, a well-posed boundary-value problem, so that the entire flow field in II may be determined. In fact, if either the streamwise or normal velocity component is specified all over $\mathcal{S}$ , together with the efflux characterization, the conditions at infinity can be used to make the problem determinate, so that it may be solved for the unspecified quantities. That is to say that in unconfined flow the values $v_x$ , $v_y$ ... at $\mathcal{S}$ bear certain functional relationships to one another, which are due to the nature of the fluid stream in II and the very strong condition that it is unconfined. The presence of the propulsion-system efflux in II complicates the equations of motion in that region and a key task is to develop a suitable representation for this imbedded high-energy flow. Neverthless, with such a representation, the equations of motion in the remainder of II are those of inviscid flow, for which many powerful analytical techniques are available.

Now, on the other hand, let us consider the flow field in I. Conditions well upstream of the model are fixed, i.e., uniform. The flow in I is determined by the model configuration together with the condition that the unconfined-flow functional relationships are satisfied at $\mathcal{S}$ . These relationships constitute the statement of the unboundedness of II, so far as I is concerned.

In a wind-tunnel experiment, the control surface $\mathcal{S}$ would be located on or within the tunnel walls but need not have the shape of the tunnel. Quantities measured at $\mathcal{S}$ in a typical experimental situation would deviate from these functional relationships, and such deviation is a measure of the departure of the flow from unconfined-flow conditions. If active control of the flow by

*This boundary $\mathcal{S}$ will be referred to as a control surface in the mathematical sense of the term.

the walls is available, the flow can be adjusted until the existence of free-flight conditions within the tunnel is signalled by the fact that the proper functional relationships exist among the quantities measured at $\mathcal{S}$ .

The principle involved here may be illustrated by a simple example: suppose the flow field is one of linearized, two-dimensional, compressible, irrotational flow about an arbitrary body without propulsion-system efflux (figure 16). Under these conditions the Prandtl-Glauert equation is applicable. If, in two dimensions, we locate the ends of the control surface $\mathcal{S}$ infinitely far upstream and downstream, $\mathcal{S}$ becomes two infinite lines, here located at $z = \pm h$ . I is the region $|z| < h$ and II is the entire region $|z| > h$ . The upper and lower parts of II can be considered independently of one another. If $v_x(x,z)$ and $v_z(x,z)$ are the disturbance velocity components at any point in the flow field, then the flow will be unconfined in I if the following equations, which are equivalent (see reference 30, for example), are satisfied along the two branches of $\mathcal{S}$ ; namely

$$v_x(x, \pm h) = \mp \frac{1}{\pi\beta} \oint_{-\infty}^{\infty} \frac{v_z(x', \pm h)\, dx'}{x' - x} \tag{76}$$

$$v_z(x, \pm h) = \pm \frac{\beta}{\pi} \oint_{-\infty}^{\infty} \frac{v_x(x', \pm h)\, dx'}{x' - x} \tag{77}$$

To achieve interference-free flow in I, $v_x$ and $v_z$ are measured along the control surfaces, say by means of the static pressure and flow inclination. Then, active wall control of the flow is applied until equations (76) and (77) are found to be satisfied to a suitable degree of accuracy on the control surfaces at $z = \pm h$ . The flow conditions in I are then unconfined.

The logic of the self-correcting wind tunnel scheme is contained in the flow chart of figure 17. Basically, the scheme is an iterative one as shown. First, a flow field is set up and the disturbance velocity components, $v_{x_m}$ and $v_{z_m}$ , say, are measured along the control surfaces. The functional relationships in II are then evaluated to determine those distributions along $\mathcal{S}$

of $v_{z_c}\,[v_{x_m}]$, say, that are consistent with the measured distributions of $v_{x_m}$ if the flow is unconfined; that is, equations (77) are evaluated. If $v_{z_c}$ does not agree with $v_{z_m}$, then the flow in I is still constrained by the walls and active wall control must be applied again. The iteration continues until $v_{z_c}$ and $v_{z_m}$ agree to within some specified accuracy. Then the flow about the model, i.e., in I, is unconfined and the desired aerodynamic data can be measured.

As an equivalent alternative to the logic of figure 17, the roles of $v_x$ and $v_z$ can be reversed. That is, we could evaluate, using equations (76), those distributions along $\mathcal{S}$ of $v_{x_c}\,[v_{z_m}]$ that are consistent with the measured distributions of $v_{z_m}$ for unconfined flow. If $v_{x_c}$ does not agree with $v_{x_m}$, then the flow is not unconfined and readjustment of the wall conditions must be continued until $v_{x_c}$ and $v_{x_m}$ agree.

The example of figure 16 is simplified from the V/STOL case, of course, because there is no propulsion-system efflux passing through the lower control surface. Although the two-dimensional functional relationships of equations (76) and (77) would remain unchanged at the upper control surface if this occurred, the functional relationships at the lower control surface would change significantly to account for the efflux.

The concept of a self-correcting wind tunnel thus embodies the following considerations. Unconfined flow about an arbitrary V/STOL configuration certainly cannot be calculated with sufficient accuracy that wind-tunnel testing can be eliminated. On the other hand, the boundaries of a wind tunnel can cause so much interference with the flow about a model that the test results may be in question, especially at very low free-stream speeds. Although the flow field in the vicinity of the model cannot be predicted analytically, the flow field external to the control surface is represented by a well-posed boundary-value problem that is within the capability of existing analytical and computational techniques. Therefore, by combining theory and experiment in a way that uses each to its best advantage, the self-correcting wind tunnel will permit simulation of free-flight conditions in the flow about the model.

# APPENDIX

## Ground Effect

The same basic principles would hold if it were desired to determine the effect of the ground on a wind-tunnel model in a self-correcting wind tunnel. In fully unconfined flow, the flow disturbance quantities must vanish at an infinite distance in all directions from the model and its trailing vortex wake. In the presence of the ground, however, the disturbances must vanish far away from the model and its wake in all directions except below the model where the flow velocity normal to the ground must be zero everywhere along the ground plane. For ground simulation in a self-correcting wind tunnel, the control surface must be entirely above the desired ground-plane location. Then the external-flow functional relationships in ground effect can be derived in a similar fashion to those for fully unconfined flow providing that the normal-flow boundary condition is applied at the ground location.

## REFERENCES


1. Mort, K.W.; Kelly, M.W.; and Hickey, D.H.: The Rationale and Design Features for the 40-by 80-/80-by 120-Foot Wind Tunnel. Paper No. 9 AGARD Conference Proceedings No. 174 on Windtunnel Design and Testing Techniques (London, England), 6-8 Oct. 1975.

2. Rae, W.H., Jr.: Limits on Minimum Speed V/STOL Wind-Tunnel Tests. Journal of Aircraft, vol. 4, no. 3, May-June 1967, pp. 249-254.

3. Rae, W.H., Jr.; and Shindo, S.: Comments on V/STOL Wind Tunnel Data at Low Forward Speeds. Proceedings Third Calspan/AVLABS Symposium on Aerodynamics of Rotary Wing and V/STOL Aircraft, vol. II, Buffalo, N.Y., June 1969.

4. Rae, W.H., Jr.; and Shindo, S.: An Experimental Investigation of Wind Tunnel Wall Corrections and Test Limits for V/STOL Vehicles. University of Washington, Department of Aeronautics and Astronautics Report 73-2, July 12, 1973, AD764255.

5. Lazzeroni, F.A.; and Carr, L.W.: Problems Associated with Wind Tunnel Tests of High Disk Loading Systems at Low Forward Speeds. Proceedings Third Calspan/AVLABS Symposium on Aerodynamics of Rotary Wing and V/STOL Aircraft, vol. II, Buffalo, N.Y., June 1969.

6. Tyler, R.A.; and Williamson, R.G.: Experience with the NRC 10 Ft. x 20 Ft. V/STOL Propulsion Tunnel - Some Practical Aspects of V/STOL Engine Model Testing. Canadian Aeronautics and Space Journal, vol. 18, no. 9, Sept. 1972, pp. 191-199.

7. Wickens, R.; South, P.; et al: Experimental Developments in V/STOL Wind Tunnel Testing at the National Aeronautical Establishment. Canadian Aeronautics and Space Journal, vol. 19, no. 4, April 1973, pp. 145-154.

8. Cull, M.J.: V/STOL Wind Tunnel Model Testing: An Experimental Assessment of Flow Breakdown Using a Multiple Fan Model. Paper No. 43, AGARD Conference Proceedings No. 174 on Windtunnel Design and Testing Techniques (London, England), 6-8 Oct. 1975.

9. Heyson, H.H.: Jet-Boundary Corrections for Lifting Rotors Centered in Rectangular Wind Tunnels. NASA TR R-71, 1960.

10. Heyson, H.H.: Linearized Theory of Wind-Tunnel Jet-Boundary Corrections and Ground Effect for VTOL-STOL Aircraft. NASA TR R-124, 1962.

11. Heyson, H.H.: The Flow Throughout a Wind Tunnel Containing a Rotor with a Sharply Deflected Wake. Proceedings Third Calspan/AVLABS Symposium on Aerodynamics of Rotary Wing and V/STOL Aircraft, vol. II, Buffalo, N.Y., June 1969.

12. Heyson, H.H.: General Theory of Wall Interference for Static Stability Tests in Closed Rectangular Sections and in Ground Effect. NASA TR R-364, 1971.

13. Lo, C.F.; and Binion, T.W., Jr.: A V/STOL Wind-Tunnel Wall Interference Study. Journal of Aircraft, vol. 7, no. 1, Jan.-Feb. 1970, pp. 51-57.

14. Lo. C.F.: Wind-Tunnel Boundary Interference on a V/STOL Model. Journal of Aircraft, vol. 8, no. 3, March 1971, pp. 162-167.

15. Lo, C.F.: Test Section for a V/STOL Wind Tunnel. Journal of Aircraft, vol. 7, no. 4, July-Aug. 1970, pp. 380-382.

16. Kraft, E.M.; and Lo, C.F.: A General Solution for Lift Interference in Rectangular Ventilated Wind Tunnels. AIAA Paper No. 73-209, Jan. 1973.

17. Kraft, E.M.: Analytical Study of Ventilated Wind Tunnel Boundary Interference on V/STOL Models Including Wake Curvature and Decay Effects. Air Force AEDC-TR-74-51, Nov. 1974.

18. Joppa, R.G.: Wind Tunnel Interference Factors for High-Lift Wings in Closed Wind Tunnels. NASA-CR-2191, Feb. 1973.

19. Heyson, H.H.: Theoretical Study of the Use of Variable Geometry in the Design of Minimal-Correction V/STOL Wind Tunnels. NASA TR-R-318, 1969.

20. Wright, R.H.: Test Sections for Small Theoretical Wind-Tunnel-Boundary Interference on V/STOL Models. NASA TR R-286, 1968.

21. Kroeger, R.A.; and Martin, W.A.: The Streamline Matching Technique for V/STOL Wind Tunnel Corrections. AIAA Paper No. 67-183, Jan. 1967.

22. Kroeger, R.A.: Wind Tunnel Design for Testing V/STOL Aircraft in Transition Flight. Air Force, AEDC TR-72-119, Sept. 1972.

23. Binion, T.W., Jr.: An Investigation of Several Slotted Wind Tunnel Wall Configurations with a High Disc Loading V/STOL Model. Air Force AEDC TR-71-77, 1971.

24. Binion, T.W., Jr.: An Experimental Study of Several Wind Tunnel Wall Configurations Using Two V/STOL Model Configurations. Report No. AEDC-TR-75-36, Arnold Engineering Development Center, July 1975.

25. Grunwald, K.J.: Experimental Investigation of the Use of Slotted Test-Section Walls to Reduce Wall Interference for High-Lift-Model Testing. NASA TN D-6292, 1971.

26. Parker, A.G.: Use of Slotted Walls to Reduce Wind-Tunnel Boundary Corrections in Subsonic Flow. AIAA Journal, vol. 12, no. 12, Dec. 1974, pp. 1771-1772.

27. Bernstein, S.; and Joppa, R.G.: Development of Minimum Correction Wind Tunnels. J. Aircraft, vol. 12, no. 4, April 1976, pp. 243-247.

28. Bernstein, S.; and Joppa, R.G.: Reduction of Wind Tunnel Wall Interference by Controlled Wall Flow. NASA-CR-2654, March 1976.

29. Sears, W.R.: Self-Correcting Wind Tunnels. (The Sixteenth Lanchester Memorial Lecture). The Aeronautical Journal, vol. 78, no. 758/759, Feb./March 1974, pp. 80-89; also Calspan Reports Nos. RK-5070-A-2, July 1973 and RK-5070-A-4, Oct. 1975.

30. Erickson, J.C., Jr.; and Nenni, J.P.: A Numerical Demonstration of the Establishment of Unconfined-Flow Conditions in a Self-Correcting Wind Tunnel. Calspan Report No. RK-5070-A-1, Nov. 1973.

31. Vidal, R.J.; Erickson, J.C., Jr.; and Catlin, P.A.: Experiments with a Self-Correcting Wind Tunnel. Paper No. 11, AGARD Conference Proceedings No. 174 on Windtunnel Design and Testing Techniques (London, England), 6-8 Oct. 1975.

32. Ferri, A; and Baronti, P.: A Method for Transonic Wind Tunnel Corrections. AIAA J., vol. 11, no. 1, Jan. 1973, pp. 63-66.

33. Weeks, T.M.: Reduction of Transonic Slotted Wall Interference by Means of Slat Contouring. Report No. AFFDL-TR-74-139, Air Force Flight Dynamics Laboratory, March 1975.

34. Goodyer, M.J.: A Low Speed Self Streamlining Wind Tunnel. Paper No. 13, AGARD Conference Proceedings No. 174 on Windtunnel Design and Testing Techniques (London, England), 6-8 Oct. 1975.

35. Goodyer, M.J.: The Self Streamlining Wind Tunnel. NASA-TM-X-72699, Aug. 1975.

36. Chevallier, J.P.: Soufflerie Transsonique a Parois Auto-Adaptables. Paper No. 12, AGARD Conference Proceedings No. 174 on Windtunnel Design and Testing Techniques (London, England), 6-8 Oct. 1975.

37. Hess, J.L.; and Smith, A.M.O.: Calculation of Non-Lifting Potential Flow About Arbitrary Three-Dimensional Bodies. Douglas Aircraft Report No. E.S. 40622, 15 March 1962.

38. Hess, J.L.; and Smith, A.M.O.: Calculation of Potential Flow About Arbitrary Bodies. Progress in Aeronautical Sciences, vol. 8, 1967, pp. 1-138, Pergamon Press.

39. Hess, J.L.: Review of Integral-Equation Techniques for Solving Potential-Flow Problems with Emphasis on the Surface-Source Method. Computer Methods in Applied Mechanics and Engineering, vol. 5, 1975, pp. 145-196.

40. Pindzola, M.; and Lo. C.F.: Boundary Interference at Subsonic Speeds in Wind Tunnels with Ventilated Walls. AEDC Report No. AEDC-TR-69-47, May 1969.

41. Hough, G.R.: Remarks on Vortex-Lattice Methods. Journal of Aircraft, vol. 10, no. 5, May 1973, pp. 314-317.

42. Milne-Thomson, L.M.: Theoretical Hydrodynamics. Fifth Edition, The Macmillan Company, 1968.

43. Durand, W.F., Editor: Aerodynamic Theory, vol. II, pp. 143-146, Dover Publications, Inc., New York, 1963.

44. Lotz, I.: Corrections of Downwash in Wind Tunnels of Circular and Elliptic Sections. NACA TM No. 801, July 1936.

45. Sears, W.R.: Small Perturbation Theory. Vol. 6 of High Speed Aerodynamics and Jet Propulsion, General Theory of High Speed Aerodynamics, Section C, W.R. Sears, ed., Princeton U. Press (Princeton), 1954, pp. 69-71.

46. Vidal, R.J.; and Rae, W.J.: On the Wall Boundary Condition for Wind Tunnels with Ventilated Test Sections. Submitted for publication.

TABLE I

MULTIPOLE VELOCITY COMPONENTS - ORIGINAL FORM OF MPE

$$\mathcal{V}_{x_1}(x,\theta;\beta) = \frac{x}{D^3} \qquad \mathcal{V}_{y_1}(x,\theta;\beta) = \beta\,\mathcal{V}_{x_{10}}(x,\theta;\beta) \qquad \mathcal{V}_{z_1}(x,\theta;\beta) = \beta\,\mathcal{V}_{x_2}(x,\theta;\beta)$$

$$\mathcal{V}_{x_2}(x,\theta;\beta) = \frac{\hat{z}}{D^3} \qquad \mathcal{V}_{y_2}(x,\theta;\beta) = -\frac{\beta 2\,\hat{y}\,\hat{z}\,H_1(x,D,\hat{R})}{\hat{R}^4} \qquad \mathcal{V}_{z_2}(x,\theta;\beta) = \frac{\beta(\hat{y}^2-\hat{z}^2)\,H_1(x,D,\hat{R})}{\hat{R}^4} - \frac{\beta x}{2D^3}$$

$$\mathcal{V}_{x_3}(x,\theta;\beta) = \frac{D^2-3x^2}{D^5} \qquad \mathcal{V}_{y_3}(x,\theta;\beta) = \beta\,\mathcal{V}_{x_{11}}(x,\theta;\beta) \qquad \mathcal{V}_{z_3}(x,\theta;\beta) = \beta\,\mathcal{V}_{x_4}(x,\theta;\beta)$$

$$\mathcal{V}_{x_4}(x,\theta;\beta) = -\frac{3x\hat{z}}{D^5} \qquad \mathcal{V}_{y_4}(x,\theta;\beta) = \beta\,\mathcal{V}_{x_{12}}(x,\theta;\beta) \qquad \mathcal{V}_{z_4}(x,\theta;\beta) = \beta\,\mathcal{V}_{x_5}(x,\theta;\beta)$$

$$\mathcal{V}_{x_5}(x,\theta;\beta) = \frac{D^2-3\hat{z}^2}{D^5} \qquad \mathcal{V}_{y_5}(x,\theta;\beta) = -\frac{\beta 2\,\hat{y}(\hat{y}^2-3\hat{z}^2)\,H_2(x,D,\hat{R})}{\hat{R}^6} + \frac{\beta 3x\hat{y}}{4D^5} \qquad \mathcal{V}_{z_5}(x,\theta;\beta) = -\frac{\beta 2\hat{z}(3\hat{y}^2-\hat{z}^2)\,H_2(x,D,\hat{R})}{\hat{R}^6} + \frac{\beta 9x\hat{z}}{4D^5}$$

$$\mathcal{V}_{x_6}(x,\theta;\beta) = \frac{x(3D^2-5x^2)}{D^7} \qquad \mathcal{V}_{y_6}(x,\theta;\beta) = \beta\,\mathcal{V}_{x_{13}}(x,\theta;\beta) \qquad \mathcal{V}_{z_6}(x,\theta;\beta) = \beta\,\mathcal{V}_{x_7}(x,\theta;\beta)$$

$$\mathcal{V}_{x_7}(x,\theta;\beta) = \frac{\hat{z}(D^2-5x^2)}{D^7} \qquad \mathcal{V}_{y_7}(x,\theta;\beta) = \beta\,\mathcal{V}_{x_{14}}(x,\theta;\beta) \qquad \mathcal{V}_{z_7}(x,\theta;\beta) = \beta\,\mathcal{V}_{x_8}(x,\theta;\beta)$$

TABLE I (Continued)

MULTIPOLE VELOCITY COMPONENTS - ORIGINAL FORM OF MPE

$$\mathcal{V}_{x_8}(x,\theta;\beta) = \frac{x(D^2-5\hat{z}^2)}{D^7} \qquad \mathcal{V}_{y_8}(x,\theta;\beta) = \beta\mathcal{V}_{x_{15}}(x,\theta;\beta) \qquad \mathcal{V}_{z_8}(x,\theta;\beta) = \beta\mathcal{V}_{x_9}(x,\theta;\beta)$$

$$\mathcal{V}_{x_9}(x,\theta;\beta) = \frac{\hat{z}(3D^2-5\hat{z}^2)}{D^7} \qquad \mathcal{V}_{y_9}(x,\theta;\beta) = -\frac{\beta 8\hat{y}\hat{z}(\hat{y}^2-\hat{z}^2)H_3(x,D,\hat{R})}{\hat{R}^8} + \frac{\beta 5 x\hat{y}\hat{z}}{2D^7} \qquad \mathcal{V}_{z_9}(x,\theta;\beta) = \frac{\beta 2(\hat{y}^4-6\hat{y}^2\hat{z}^2+\hat{z}^4)H_3(x,D,\hat{R})}{\hat{R}^8} - \frac{\beta x(6D^2+5\hat{R}^2-40\hat{z}^2)}{8D^7}$$

$$\mathcal{V}_{x_{10}}(x,\theta;\beta) = \frac{\hat{y}}{D^3} \qquad \mathcal{V}_{y_{10}}(x,\theta;\beta) = -\frac{\beta(\hat{y}^2-\hat{z}^2)H_1(x,D,\hat{R})}{\hat{R}^4} - \frac{\beta x}{2D^3} \qquad \mathcal{V}_{z_{10}}(x,\theta;\beta) = \mathcal{V}_{y_2}(x,\theta;\beta)$$

$$\mathcal{V}_{x_{11}}(x,\theta;\beta) = -\frac{3x\hat{y}}{D^5} \qquad \mathcal{V}_{y_{11}}(x,\theta;\beta) = \frac{\beta(D^2-3\hat{y}^2)}{D^5} \qquad \mathcal{V}_{z_{11}}(x,\theta;\beta) = \beta\mathcal{V}_{x_{12}}(x,\theta;\beta)$$

$$\mathcal{V}_{x_{12}}(x,\theta;\beta) = -\frac{3\hat{y}\hat{z}}{D^5} \qquad \mathcal{V}_{y_{12}}(x,\theta;\beta) = \frac{\beta 2\hat{z}(3\hat{y}^2-\hat{z}^2)H_2(x,D,\hat{R})}{\hat{R}^6} + \frac{\beta 3 x\hat{z}}{4D^5} \qquad \mathcal{V}_{z_{12}}(x,\theta;\beta) = \mathcal{V}_{y_5}(x,\theta;\beta)$$

TABLE I (Concluded)

MULTIPOLE VELOCITY COMPONENTS - ORIGINAL FORM OF MPE

$$\mathcal{V}_{x_{13}}(x,\Theta;\beta) = \frac{\hat{y}(D^2-5x^2)}{D^7} \qquad \mathcal{V}_{y_{13}}(x,\Theta;\beta) = \frac{\beta x(D^2-5\hat{y}^2)}{D^7} \qquad \mathcal{V}_{z_{13}}(x,\Theta;\beta) = \beta\mathcal{V}_{x_{14}}(x,\Theta;\beta)$$

$$\mathcal{V}_{x_{14}}(x,\Theta;\beta) = -\frac{5x\hat{y}\hat{z}}{D^7} \qquad \mathcal{V}_{y_{14}}(x,\Theta;\beta) = \frac{\beta\hat{z}(D^2-5\hat{y}^2)}{D^7} \qquad \mathcal{V}_{z_{14}}(x,\Theta;\beta) = \beta\mathcal{V}_{x_{15}}(x,\Theta;\beta)$$

$$\mathcal{V}_{x_{15}}(x,\Theta;\beta) = \frac{\hat{y}(D^2-5\hat{z}^2)}{D^7} \qquad \mathcal{V}_{y_{15}}(x,\Theta;\beta) = -\frac{\beta x(\hat{y}^4-6\hat{y}^2\hat{z}^2+\hat{z}^4)H_3(x,D,\hat{R})}{\hat{R}^8} \qquad \mathcal{V}_{z_{15}}(x,\Theta;\beta) = \mathcal{V}_{y_9}(x,\Theta;\beta)$$

$$-\frac{\beta x(2D^2-5\hat{R}^2)}{8D^7}$$

where: $D^2 = -x^2+\hat{R}^2$

$$\hat{R}^2 = \hat{y}^2+\hat{z}^2$$

$$\hat{y} = \beta Y(\Theta)$$

$$\hat{z} = \beta Z(\Theta)$$

$$H_1(x,D,\hat{R}) = 1+\frac{x}{D}+\frac{x\hat{R}^2}{2D^3}$$

$$H_2(x,D,\hat{R}) = H_1(x,D,\hat{R})+\frac{3x\hat{R}^4}{8D^5}$$

$$H_3(x,D,\hat{R}) = H_2(x,D,\hat{R})+\frac{5x\hat{R}^6}{16D^7}$$

TABLE II

COMPARISON OF RMS ERRORS IN FITTED AND CALCULATED VELOCITY COMPONENTS FOR ELLIPTICALLY-LOADED WINGS BY ORIGINAL AND MODIFIED MPE,

$M_\infty = 0$, $b/a = 0.5$

| RMS Error in | Original MPE | Modified MPE | | |
|---|---|---|---|---|
| | $b_w/a$ | $b_w/a$ | | |
| | 0.5 | 0.5 | 0.75 | 0.875 |
| Fit to $4\pi AR\, v_{x_m}/U_\infty C_L$ | 0.05 | 0.00 | 0.02 | 0.08 |
| Fit to $4\pi AR\, v_{n_m}/U_\infty C_L$ | 0.15 | 0.01 | 0.08 | 0.25 |
| $4\pi AR\, v_{x_c}[v_{n_m}]/U_\infty C_L$ | 0.07 | 0.00 | 0.03 | 0.08 |
| $4\pi AR\, v_{n_c}[v_{x_m}]/U_\infty C_L$ | 0.21 | 0.01 | 0.09 | 0.27 |
| $4\pi AR\, v_{t_c}[v_{x_m}]/U_\infty C_L$ | 0.10 | 0.01 | 0.09 | 0.26 |
| $4\pi AR\, v_{t_c}[v_{n_m}]/U_\infty C_L$ | 0.15 | 0.01 | 0.08 | 0.25 |

TABLE III

EFFECT OF ERRORS IN FUNCTIONAL RELATIONSHIP EVALUATIONS BY ORIGINAL MPE ON LIFT COEFFICIENT OF ELLIPTICALLY-LOADED WINGS,

$M_\infty = 0$, $b/a = 1.0$

| | | $\Delta_x C_L / C_L$ | | | | $\Delta_n C_L / C_L$ | | |
|---|---|---|---|---|---|---|---|---|
| $b_w/a$ | $X_2/C_2$ | $AR = 1$ | 5 | 10 | $N_2/C_2$ | $AR = 1$ | 5 | 10 |
| 0.2 | 0.9986 | 0.000 | 0.000 | 0.000 | 0.9986 | 0.000 | 0.000 | 0.000 |
| 0.4 | 0.9989 | 0.000 | 0.000 | 0.000 | 1.0006 | 0.000 | 0.000 | 0.000 |
| 0.6 | 1.0009 | 0.000 | 0.000 | 0.000 | 1.0080 | 0.001 | 0.000 | 0.000 |
| 0.8 | 1.0062 | -0.002 | -0.001 | 0.000 | 1.0285 | 0.009 | 0.003 | 0.002 |

TABLE IV

EFFECT OF ERRORS IN FUNCTIONAL RELATIONSHIP EVALUATIONS BY ORIGINAL MPE ON PRESSURE COEFFICIENT OF RANKINE SOLIDS

$M_\infty = 0$, $b/a = 1.0$, $\tau = 0.2$

| $b_b/a$ | $X_3/C_3$ | $\Delta_x (v_x/U_\infty)$ | $\Delta_x C_p/C_p$ | $N_3/C_3$ | $\Delta_n (v_x/U_\infty)$ | $\Delta_n C_p/C_p$ |
|---|---|---|---|---|---|---|
| 0.2 | 0.965 | 0.000 | 0.000 | 0.977 | 0.000 | 0.000 |
| 0.5 | 0.816 | 0.000 | 0.000 | 0.862 | 0.000 | -0.001 |
| 1.0 | 0.481 | -0.004 | 0.008 | 0.547 | 0.013 | -0.026 |

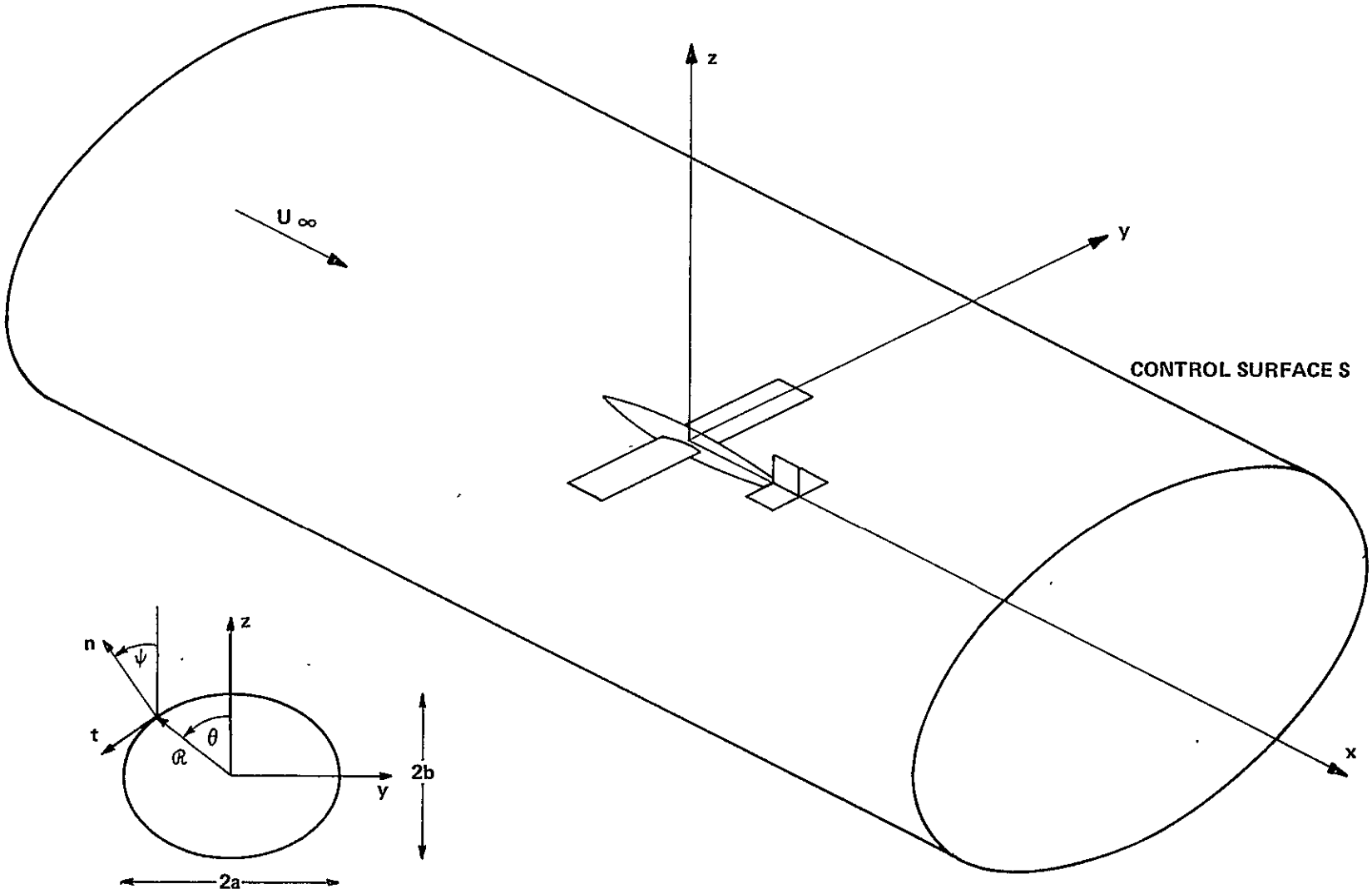


Figure 1 CONTROL-SURFACE COORDINATE SYSTEMS FOR SELF-CORRECTING WIND TUNNEL

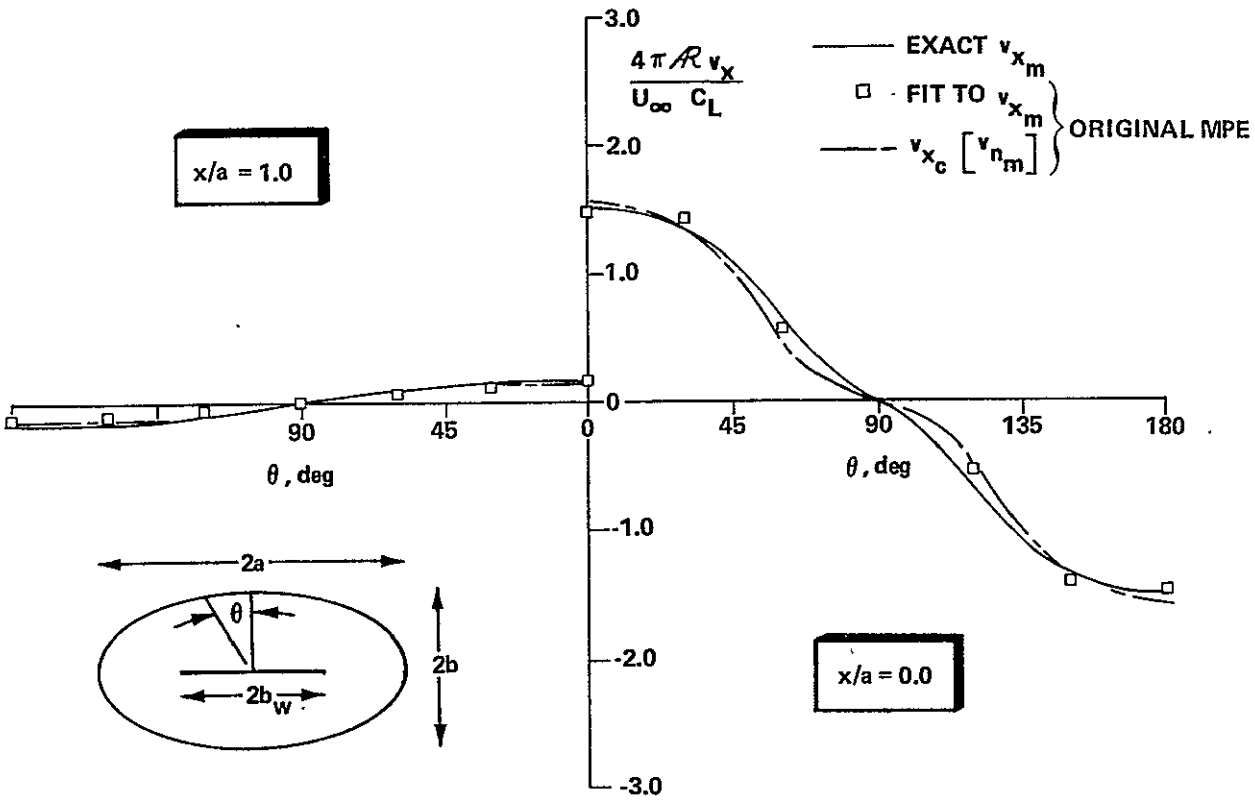


NOTE: FIT TO $v_{x_m}$ AND $v_{x_c}\left[v_{n_m}\right]$ FOR MODIFIED MPE ARE INDISTINGUISHABLE FROM $v_{x_m}$ TO THIS SCALE

Figure 2 COMPARISON OF EXACT AXIAL VELOCITY COMPONENT FOR ELLIPTICALLY-LOADED LIFTING LINE WITH RESULTS OF MPE COMPUTER PROGRAM, $M_\infty = 0$, $b/a = 0.5$, $b_w/a = 0.5$

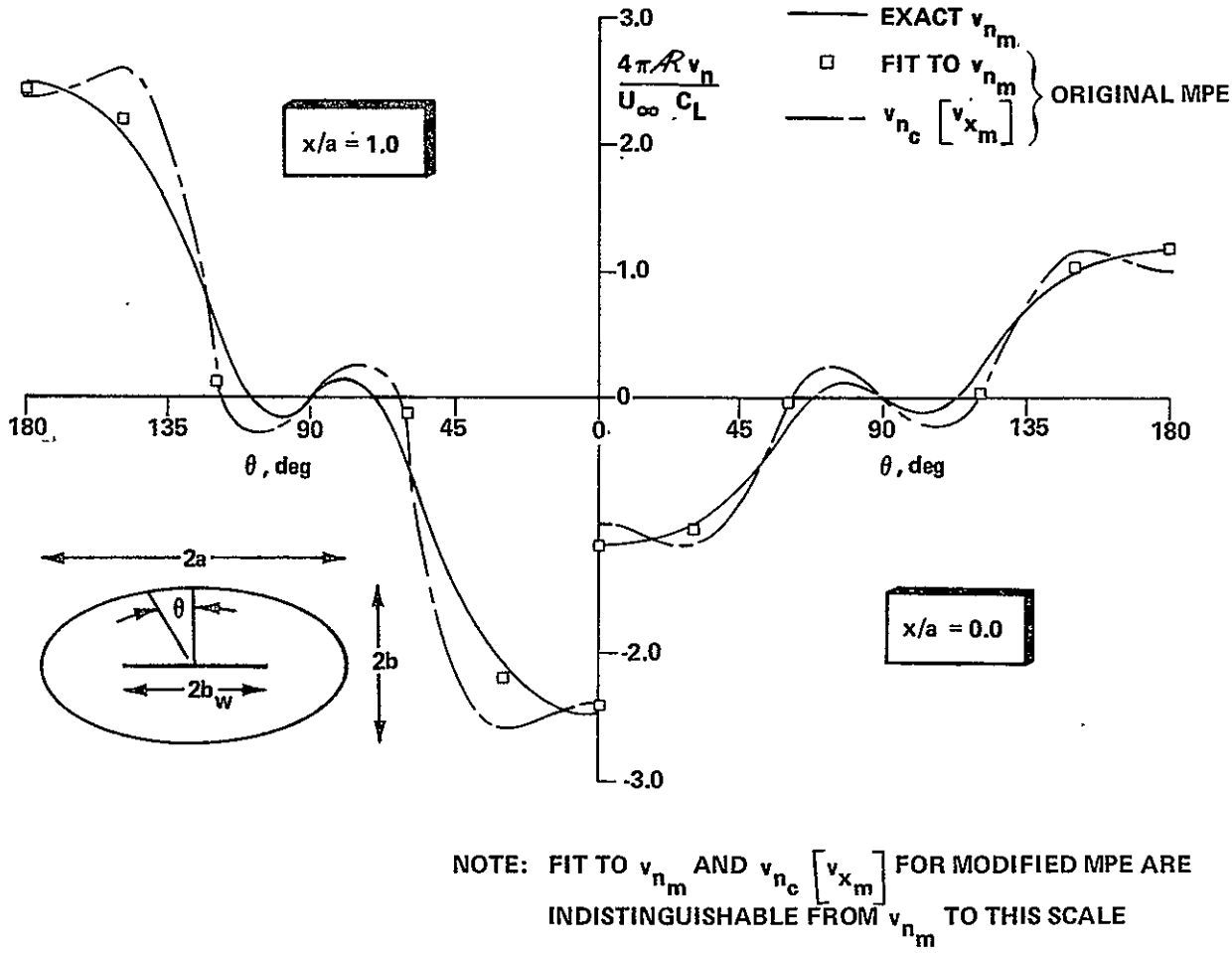


Figure 3 COMPARISON OF EXACT NORMAL VELOCITY COMPONENT FOR ELLIPTICALLY-LOADED LIFTING LINE WITH RESULTS OF MPE COMPUTER PROGRAM, $M_\infty = 0$, $b/a = 0.5$, $b_w/a = 0.5$

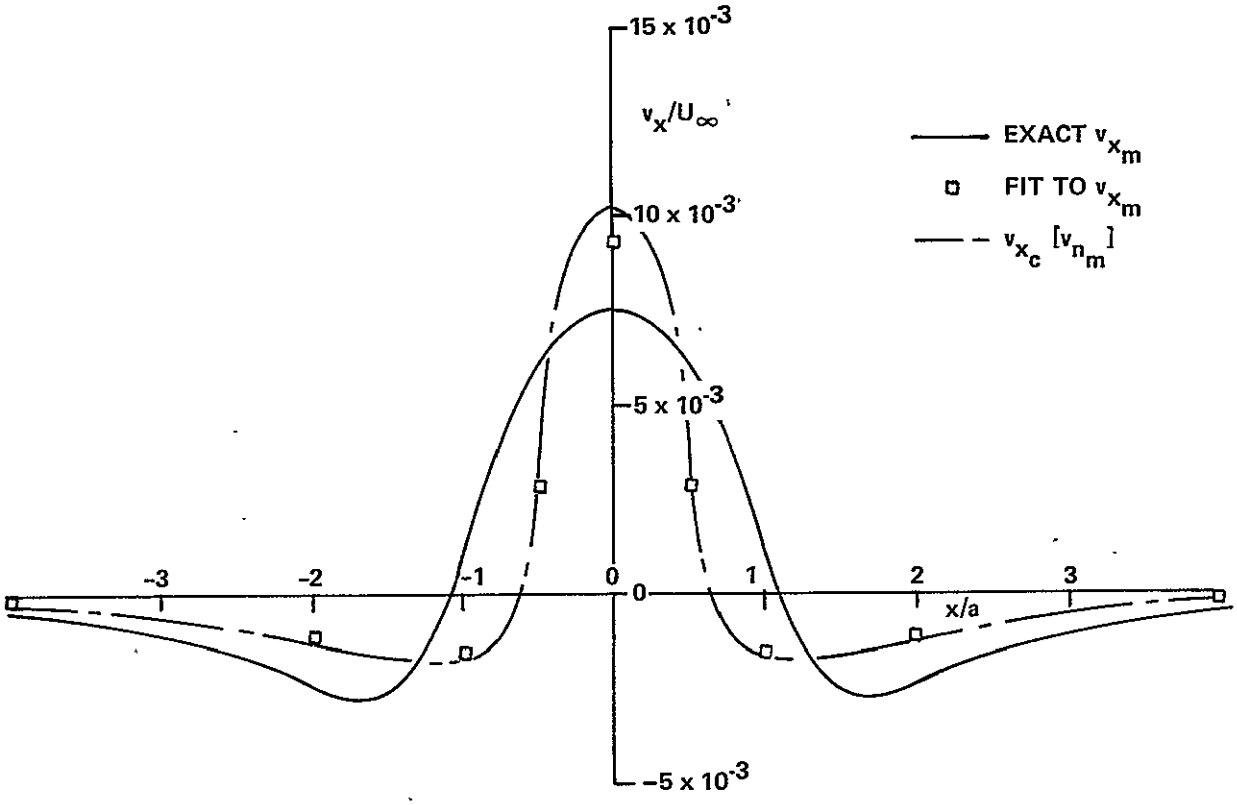


Figure 4 COMPARISON OF EXACT AXIAL VELOCITY COMPONENT FOR RANKINE SOLID WITH RESULTS OF ORIGINIAL MPE COMPUTER PROGRAM, $M_\infty$=0, b/a = 1.0, $b_b$/a = 1.0, $\tau$ = 0.2, $\Theta$ = 0

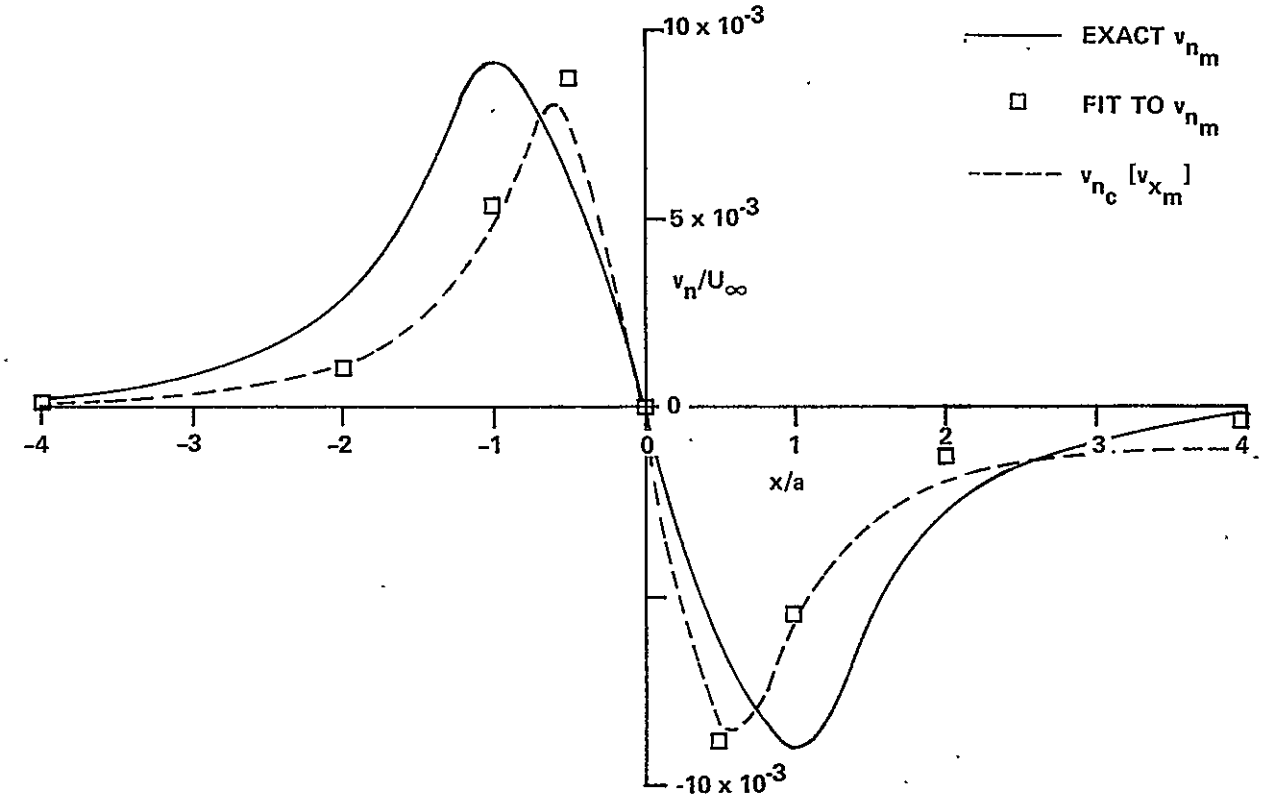


Figure 5 COMPARISON OF EXACT NORMAL VELOCITY COMPONENT FOR RANKINE SOLID WITH RESULTS OF ORIGINAL MPE COMPUTER PROGRAM, $M_\infty = 0$, b/a = 1:0 , $b_b/a = 1.0$, $\tau = 0.2$, $\Theta = 0$

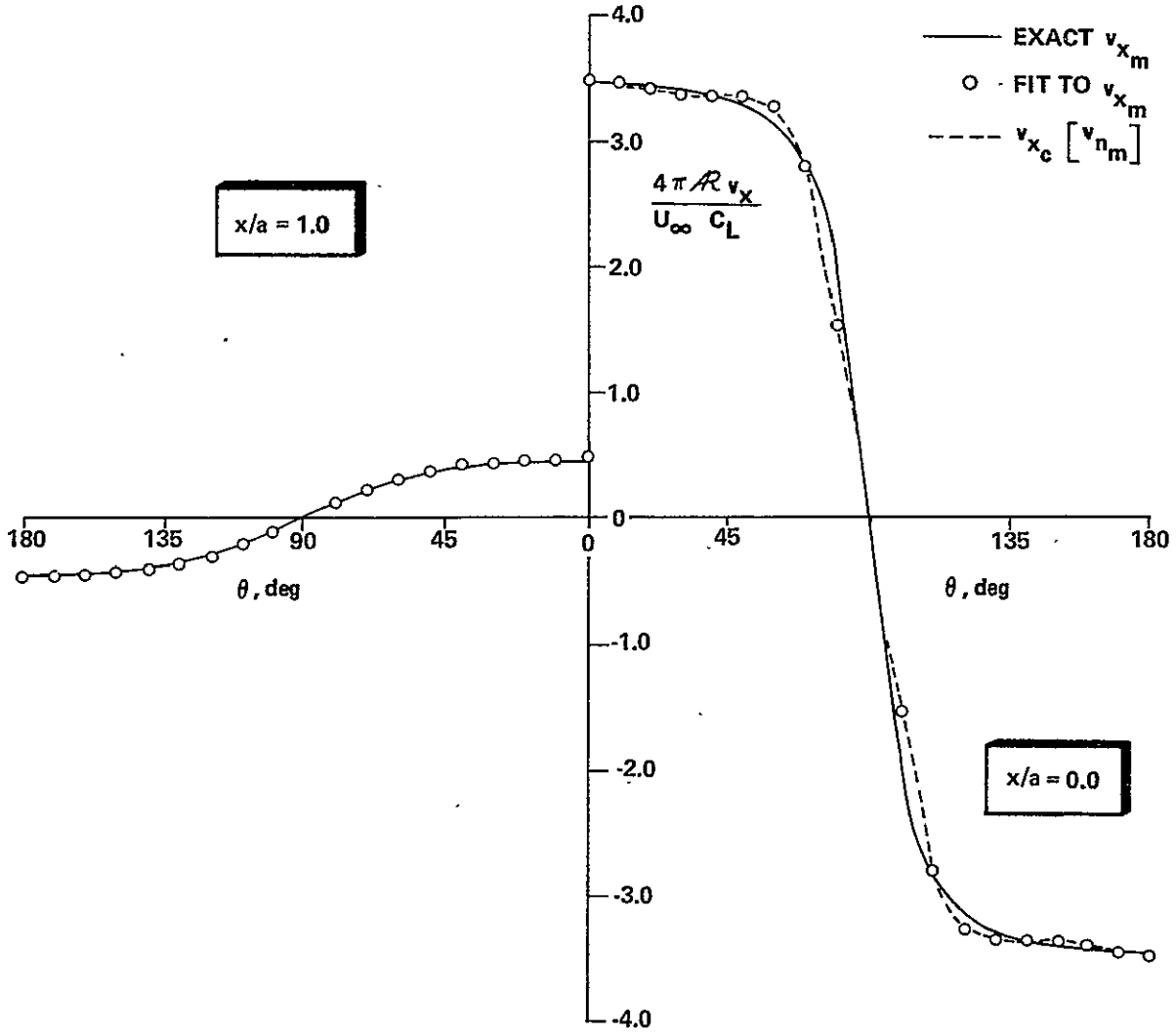


Figure 6 COMPARISON OF EXACT AXIAL VELOCITY COMPONENT FOR ELLIPTICALLY-LOADED LIFTING LINE WITH RESULTS OF MODIFIED MPE COMPUTER PROGRAM, $M_\infty = 0$, $b/a = 0.5$, $b_w/a = 0.875$

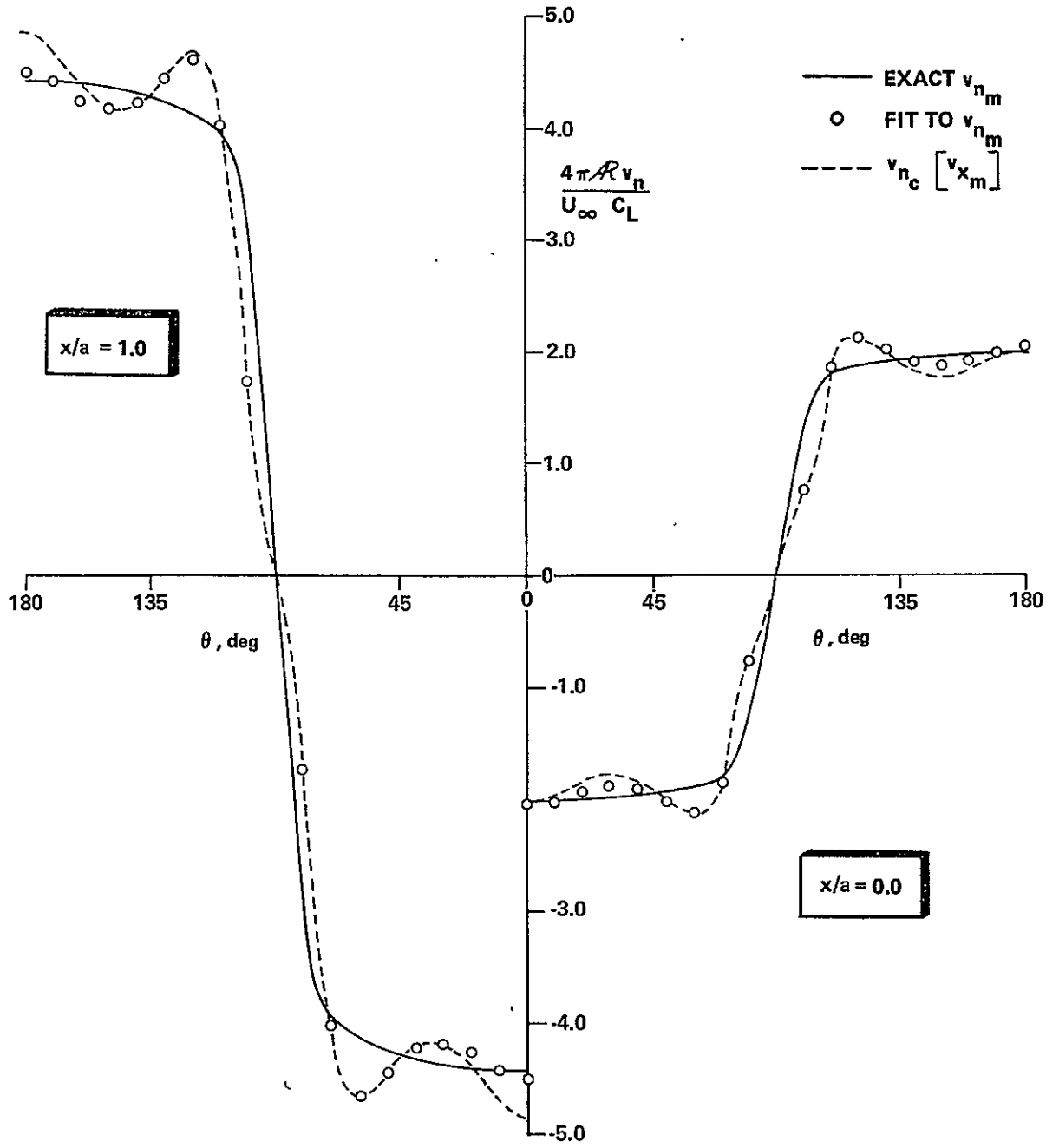


Figure 7 COMPARISON OF EXACT NORMAL VELOCITY COMPONENT FOR ELLIPTICALLY-LOADED LIFTING LINE WITH RESULTS OF MODIFIED MPE COMPUTER PROGRAM, $M_\infty = 0$, $b/a = 0.5$, $b_w/a = 0.875$

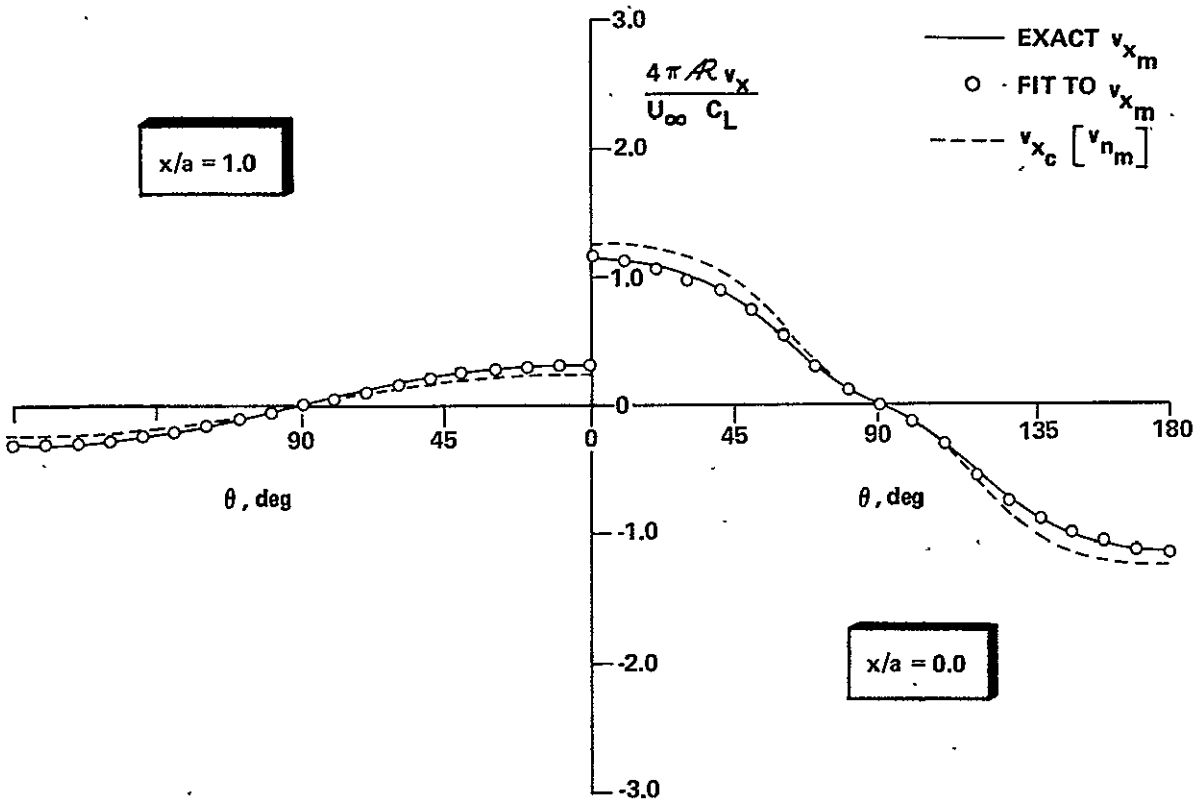


Figure 8 COMPARISON OF EXACT AXIAL VELOCITY COMPONENT FOR ELLIPTICALLY-LOADED LIFTING LINE WITH RESULTS OF MODIFIED MPE COMPUTER PROGRAM, IFTING LINE OFFSET FROM MPE ORIGIN BY $x_o/a = 0.25$, $M_\infty = 0$, $b/a = 0.5$, $_N/a = 0.5$

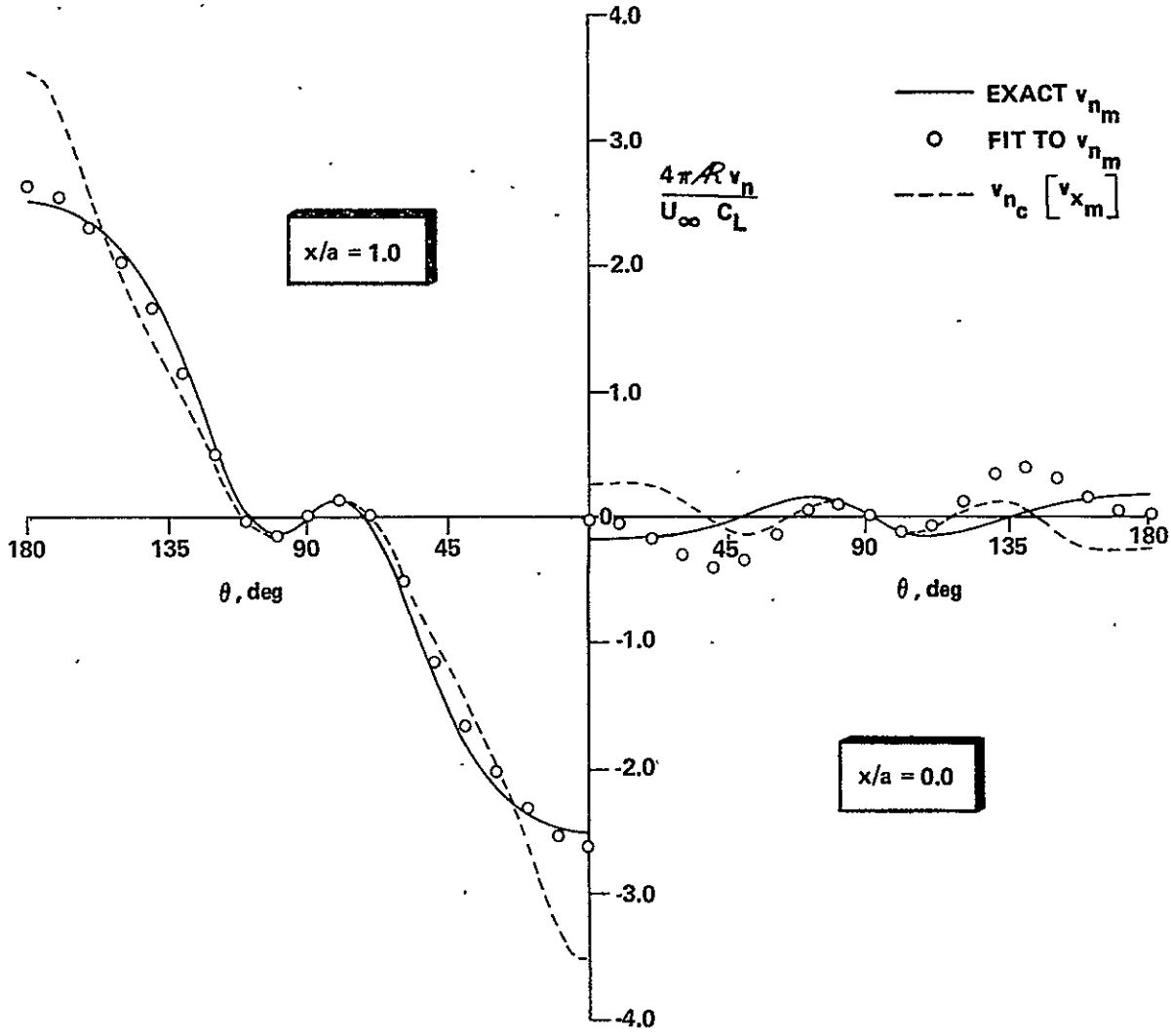


Figure 9 COMPARISON OF EXACT NORMAL VELOCITY COMPONENT FOR ELLIPTICALLY-LOADED LIFTING LINE WITH RESULTS OF MODIFIED MPE COMPUTER PROGRAM, LIFTING LINE OFFSET FROM MPE ORIGIN BY $x_o/a = 0.25$, $M_\infty = 0$, $b/a = 0.5$, $b_w/a = 0.5$

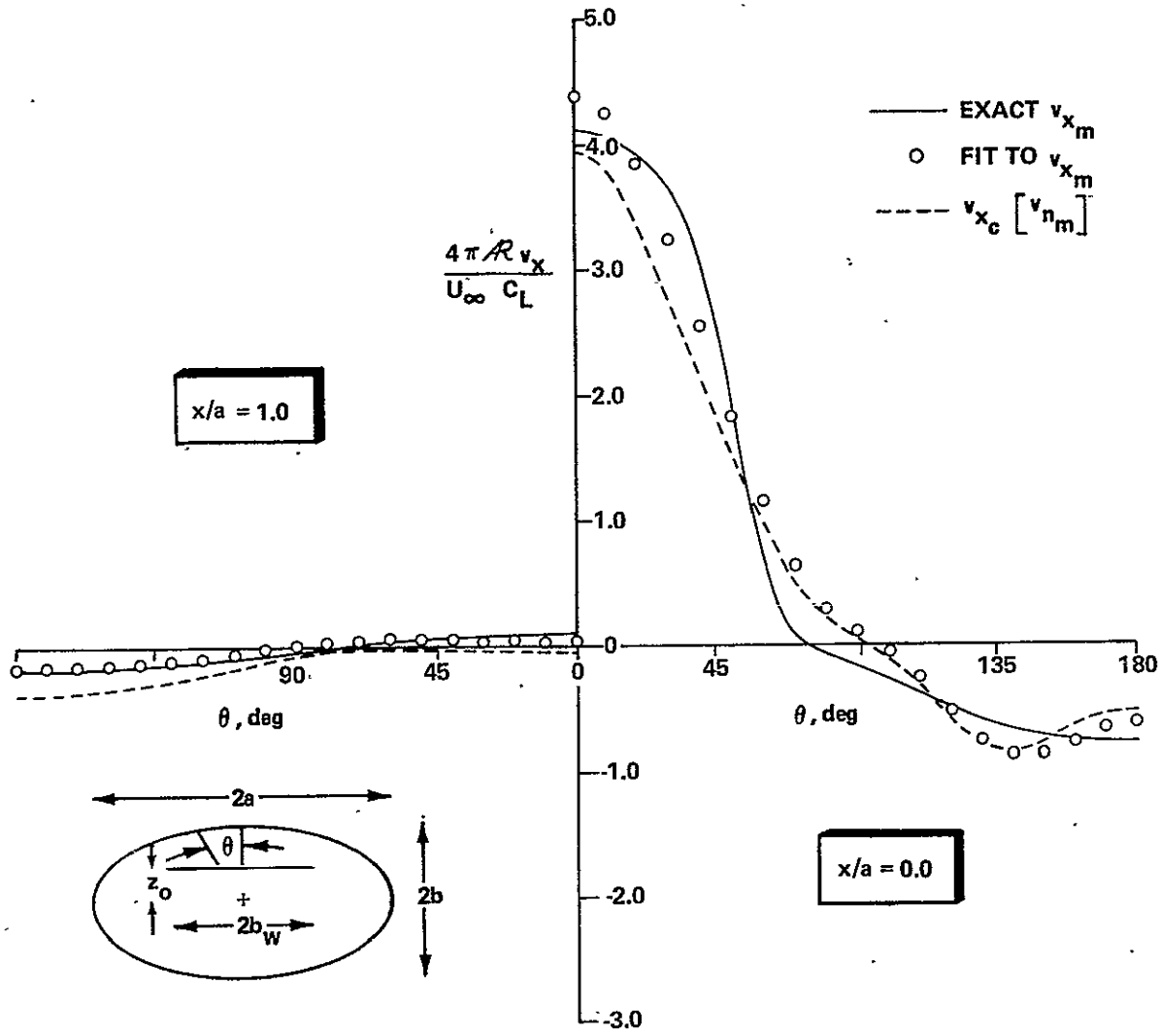


Figure 10 COMPARISON OF EXACT AXIAL VELOCITY COMPONENT FOR ELLIPTICALLY-LOADED LIFTING LINE WITH RESULTS OF MODIFIED MPE COMPUTER PROGRAM, LIFTING LINE OFFSET FROM MPE ORIGIN BY $z_o/a = 0.25$, $M_\infty = 0$, $b/a = 0.5$, $b_w/a = 0.5$

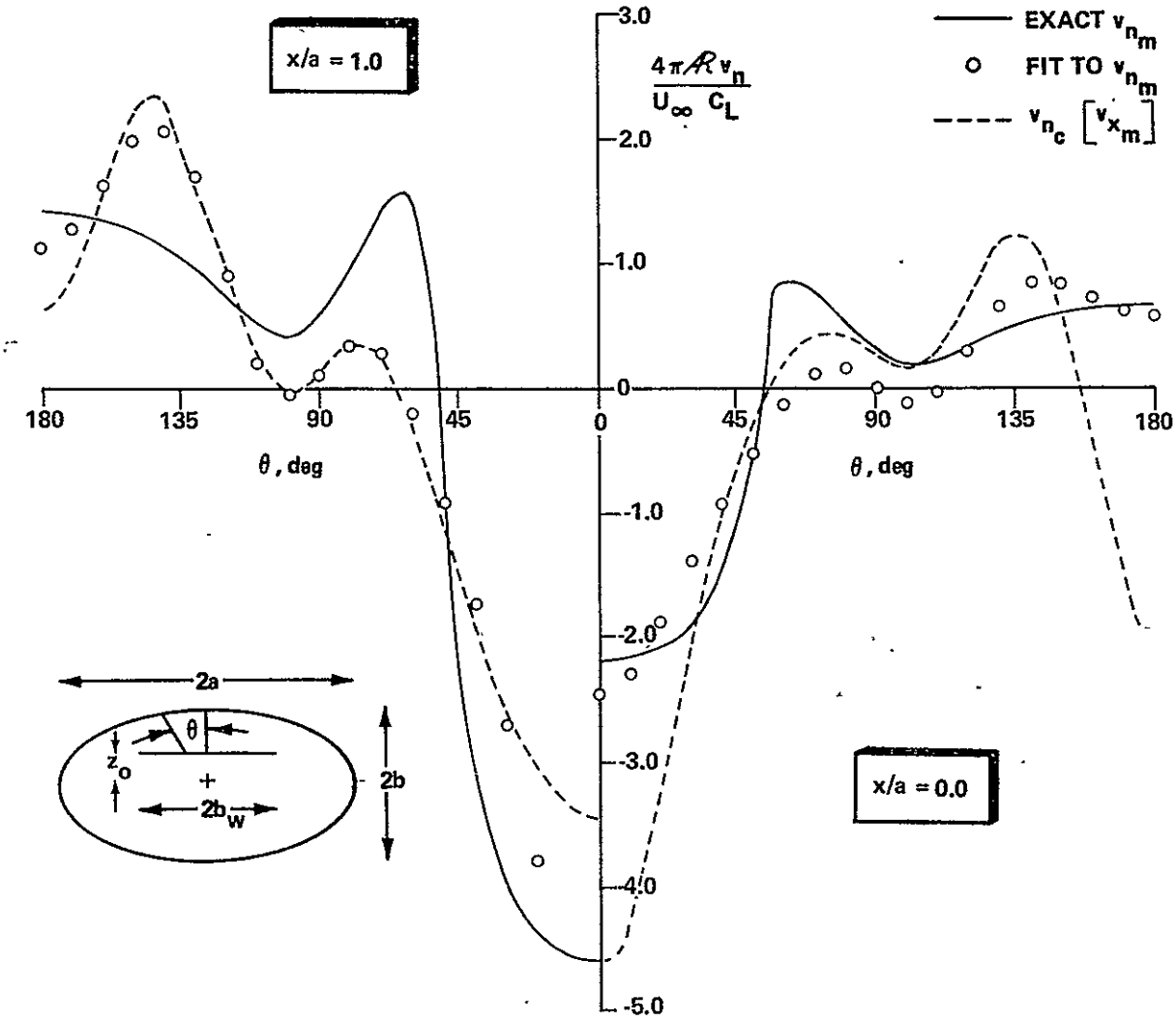


Figure 11 COMPARISON OF EXACT NORMAL VELOCITY COMPONENT FOR ELLIPTICALLY-LOADED LIFTING LINE WITH RESULTS OF MODIFIED MPE COMPUTER PROGRAM, LIFTING LINE OFFSET FROM MPE ORIGIN BY $z_o/a = 0.25$, $M_\infty = 0$, $b/a = 0.5$, $b_w/a = 0.5$

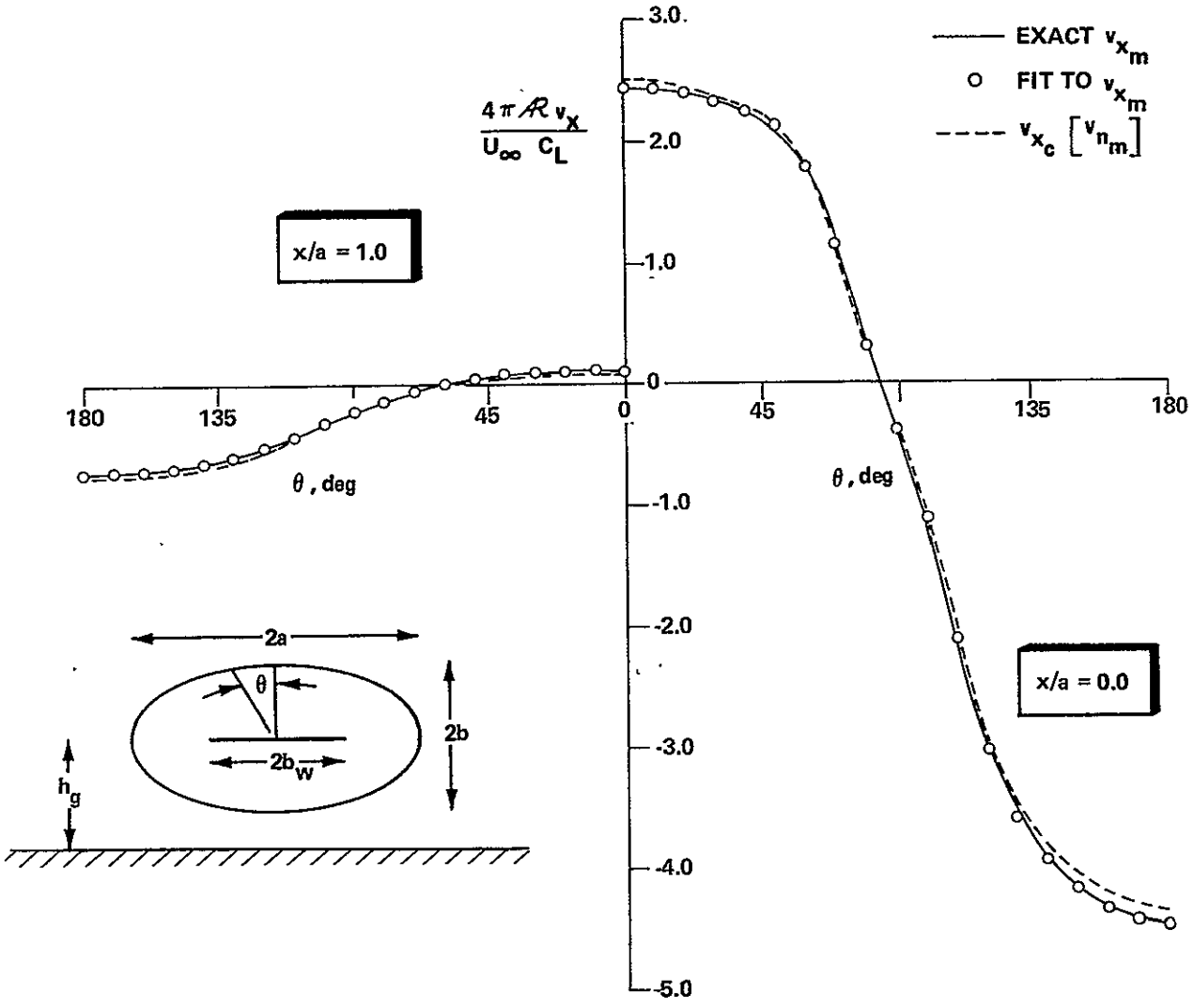


Figure 12 COMPARISON OF EXACT AXIAL VELOCITY COMPONENT FOR ELLIPTICALLY-LOADED LIFTING LINE IN GROUND EFFECT WITH RESULTS OF MODIFIED MPE COMPUTER PROGRAM, $M_\infty = 0$, $b/a = 0.5$, $b_w/a = 0.75$, $h_g/b_w = 0.8$

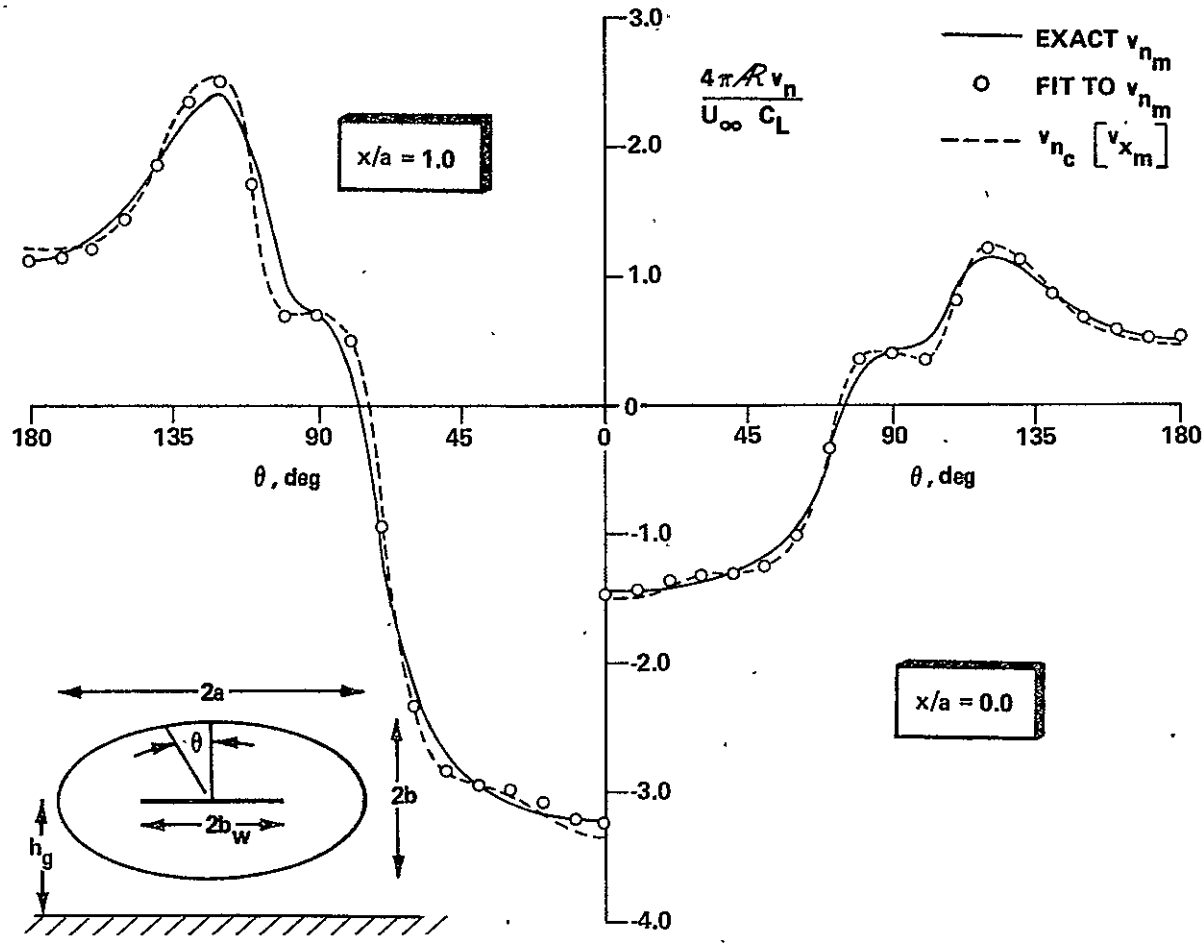


Figure 13 COMPARISON OF EXACT NORMAL VELOCITY COMPONENT FOR ELLIPTICALLY-LOADED LIFTING LINE IN GROUND EFFECT WITH RESULTS OF MODIFIED MPE COMPUTER PROGRAM, $M_\infty = 0$, $b/a = 0.5$, $b_w/a = 0.75$, $h_g/b_w = 0.8$

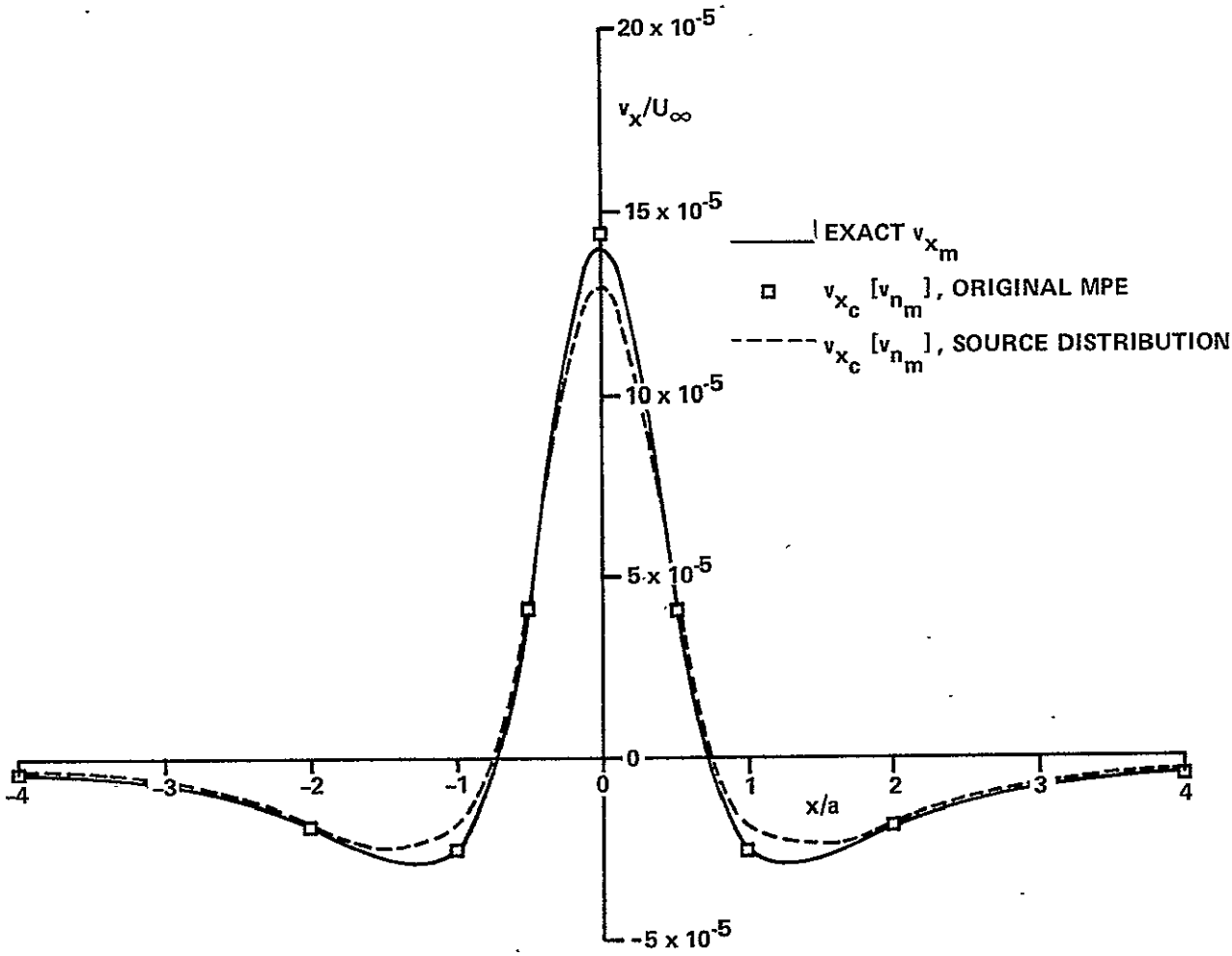


Figure 14 COMPARISON OF EXACT AXIAL VELOCITY COMPONENT FOR RANKINE SOLID WITH RESULTS OF ORIGINAL MPE COMPUTER PROGRAM AND SOURCE DISTRIBUTION PROGRAM, $M_\infty = 0$, $b/a = 1.0$, $b_b/a = 0.2$, $\tau = 0.2$, $\Theta = 0$

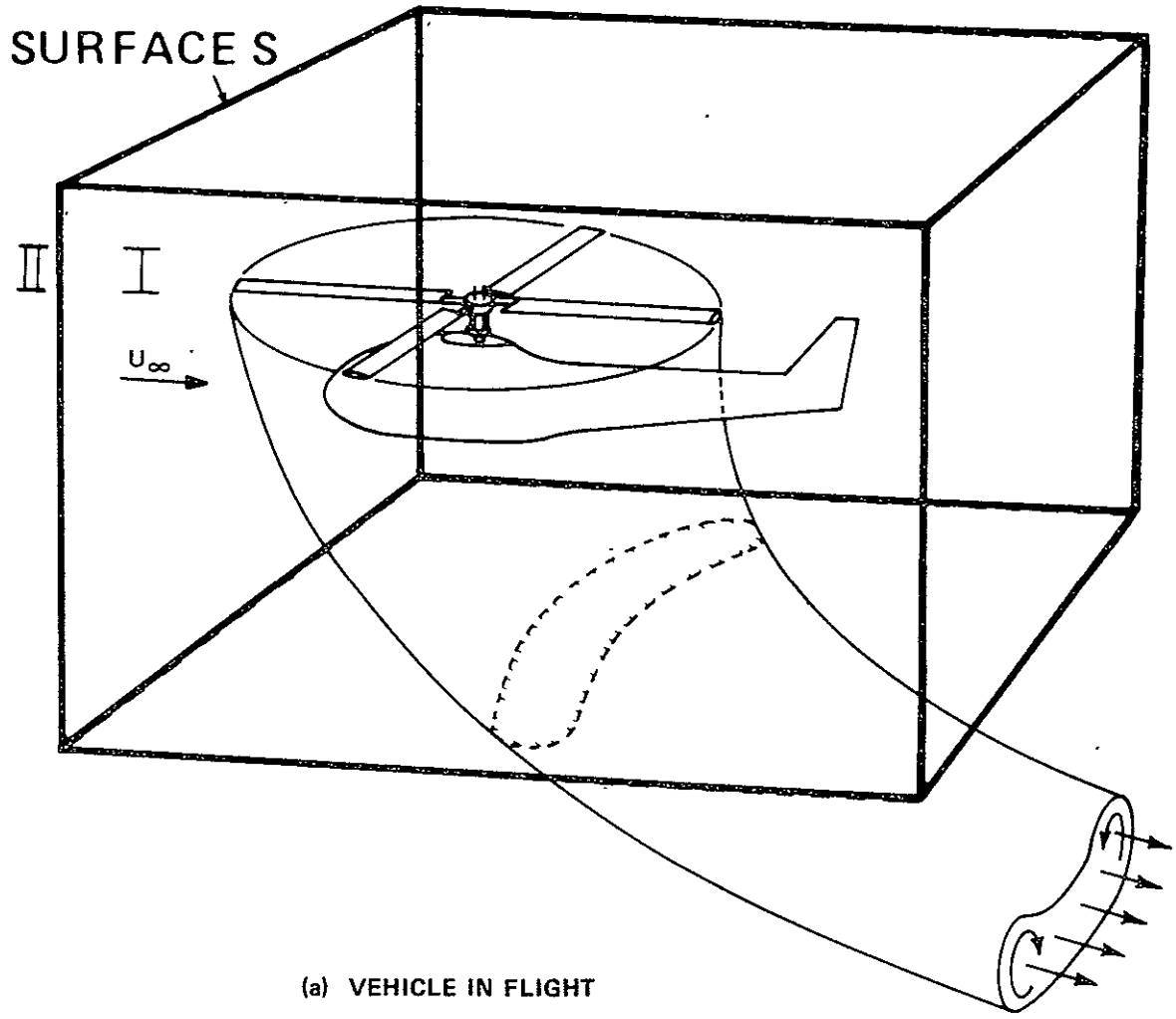


(a) VEHICLE IN FLIGHT

Figure 15 DEFINITION OF INTERIOR (I) AND EXTERIOR (II) REGIONS IN UNCONFINED FLOW ABOUT A VTOL CONFIGURATION

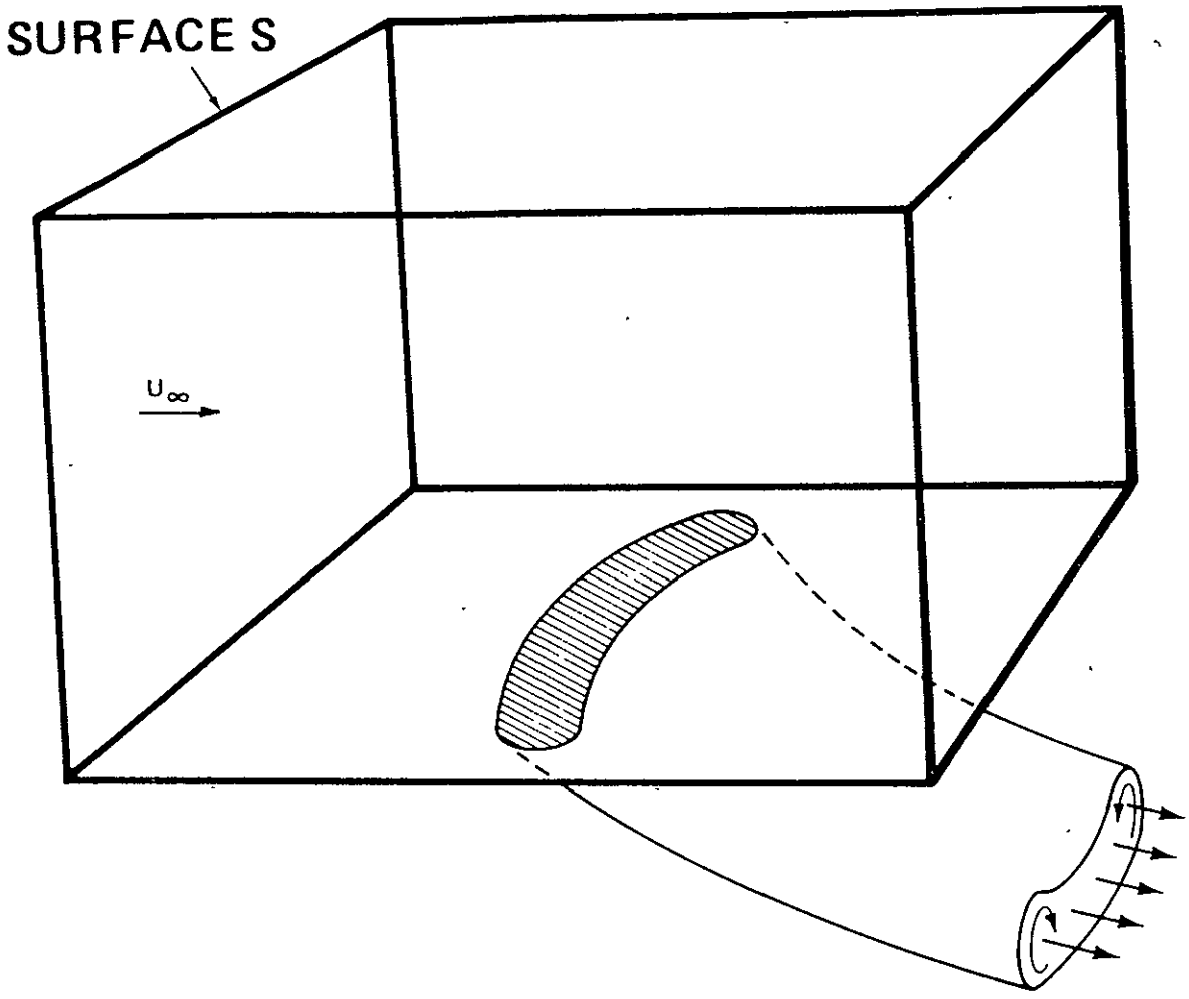


(b) FLOW IN REGION II

Figure 15 (Continued) DEFINITION OF INTERIOR (I) AND EXTERIOR (II) REGIONS IN UNCONFINED FLOW ABOUT A VTOL CONFIGURATION

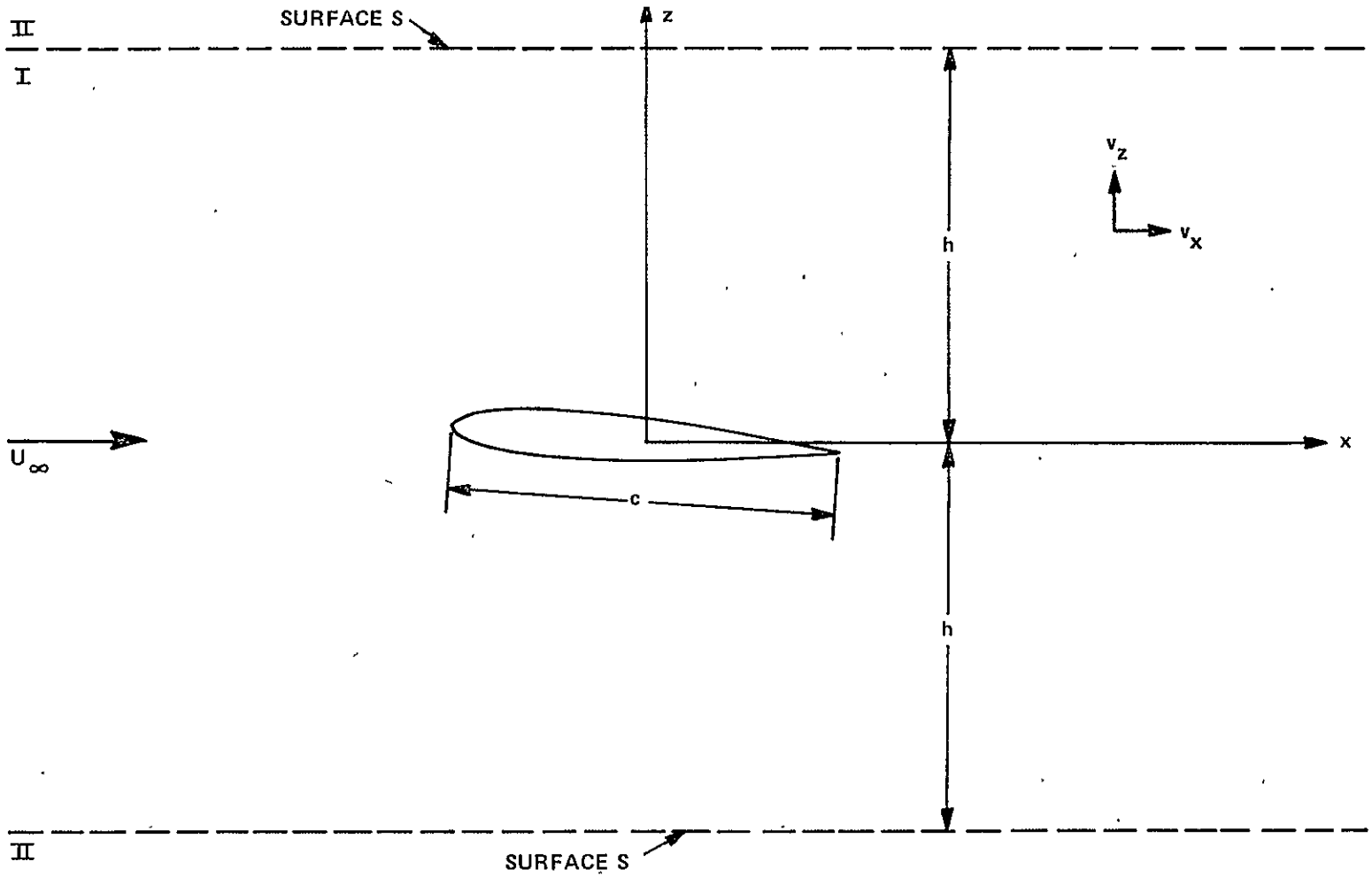


Figure 16 UNCONFINED TWO-DIMENSIONAL FLOW ABOUT AN AIRFOIL

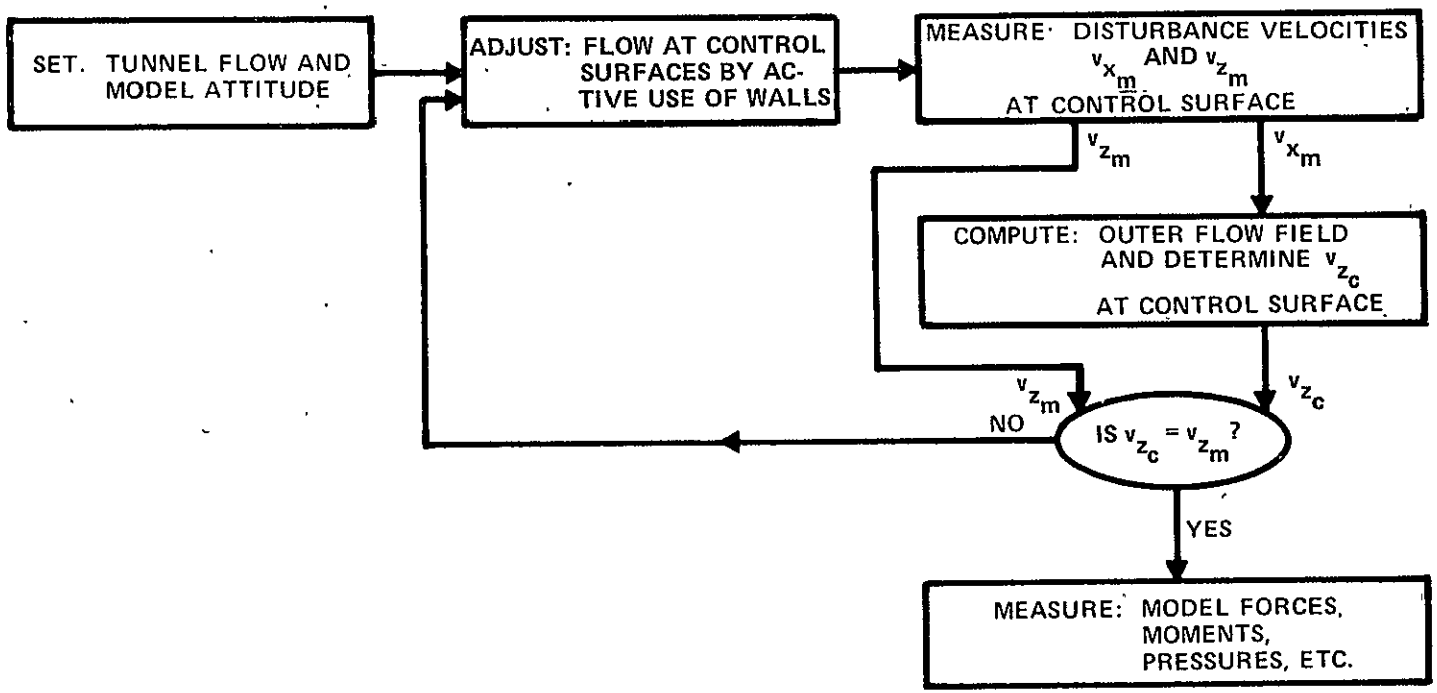


Figure 17 SELF-CORRECTING WIND TUNNEL SCHEME